eNeuro

Research Article: New Research | Cognition and Behavior

New insights from 22-kHz ultrasonic vocalizations to characterize fear responses: relationship with respiration and brain oscillatory dynamics

Maryne Dupin[1], Samuel Garcia[1], Julie Boulanger-Bertolus[1], Nathalie Buonviso[1] and Anne-Marie Mouly[1]

[1]Lyon Neuroscience Research Center, INSERM U1028; CNRS UMR5292; University Lyon1, 69366 Lyon, France

https://doi.org/10.1523/ENEURO.0065-19.2019

Received: 22 February 2019

Accepted: 23 February 2019

Published: 8 April 2019

M.D. and A.-M.M. performed research; M.D., S.G., J.B.-B., N.B., and A.-M.M. analyzed data; M.D., N.B., and A.-M.M. wrote the paper; A.-M.M. designed research.

Funding: Centre National de la Recherche Scientifique (CNRS)
;

Funding: Labex Cortex
ANR-11-LABX-0042
.

Conflict of Interest: The authors declare no competing financial interests.

This work was funded by the CNRS and the LABEX CORTEX (ANR-11-LABX-0042) of Université de Lyon, within the program “Investissements d’Avenir” (ANR-11-IDEX-0007) operated by the French National Research Agency (ANR).

Correspondence should be addressed to Maryne Dupin at maryne.dupin@inserm.fr or Anne-Marie Mouly at annemarie.mouly@cnrs.fr

Cite as: eNeuro 2019; 10.1523/ENEURO.0065-19.2019

1. Manuscript Title (50 word maximum)

New insights from 22-kHz ultrasonic vocalizations to characterize fear responses: relationship with respiration and brain oscillatory dynamics

2. Abbreviated Title (50 character maximum)

22-kHz calls, respiration, brain oscillations

3. List all Author Names and Affiliations in order as they would appear in the published article

Maryne Dupin, Samuel Garcia, Julie Boulanger-Bertolus, Nathalie Buonviso and Anne-Marie Mouly

Lyon Neuroscience Research Center, INSERM U1028; CNRS UMR5292; University Lyon1, 69366 Lyon, France

4. Author Contributions:

MD and AMM Designed Research; MD and AMM Performed research; MD, SG, JBB, NB and AMM Analyzed data; MD, NB and AMM wrote the paper.

5. Correspondence should be addressed to (include email address)

Maryne Dupin, Lyon Neuroscience Research Center, INSERM U1028; CNRS UMR5292; University Lyon1, 69366 Lyon, France. Email address: maryne.dupin@inserm.fr

Anne-Marie Mouly, Lyon Neuroscience Research Center, INSERM U1028; CNRS UMR5292; University Lyon1, 69366 Lyon, France. Email address: annemarie.mouly@cnrs.fr

6. Number of Figures : 13

7. Number of Tables : 4

8. Number of Multimedia: 0

9. Number of words for Abstract: 248

10. Number of words for Significance Statement: 120

11. Number of words for Introduction: 667

12. Number of words for Discussion: 1610

13. Acknowledgements

This work was funded by the CNRS and the LABEX CORTEX (ANR-11-LABX-0042) of Université de Lyon, within the program "Investissements d'Avenir" (ANR-11-IDEX-0007) operated by the French National Research Agency (ANR). The authors gratefully acknowledge Belkacem Messaoudi and Marc Thevenet for technical assistance, Emmanuelle Courtiol and Rémi Gervais for very valuable discussions of the data and careful reading of the manuscript, and Ounsa Ben-Hellal for taking care of the animals.

Julie Boulanger-Bertolus present address: Center for Consciousness Science, Department of Anesthesiology, University of Michigan, Ann Arbor, MI, United States.

14. Conflict of Interest

The authors declare no competing financial interests.

15. Funding sources

This work was funded by the CNRS and the LABEX CORTEX (ANR-11-LABX-0042) of Université de Lyon, within the program "Investissements d'Avenir" (ANR-11-IDEX-0007) operated by the French National Research Agency (ANR).

Abstract

Fear behavior depends on interactions between the medial prefrontal cortex (mPFC) and the basolateral amygdala (BLA), and the expression of fear involves synchronized activity in theta and gamma oscillatory activities. In addition, freezing, the most classical measure of fear response in rodents, temporally coincides with the development of sustained 4-Hz oscillations in prefrontal–amygdala circuits. Interestingly, these oscillations were recently shown to depend on the animal's respiratory rhythm, supporting the growing body of evidence pinpointing the influence of nasal breathing on brain rhythms. During fearful states, rats also emit 22-kHz ultrasonic vocalizations (USV) which drastically affect respiratory rhythm. However, the relationship between 22-kHz USV, respiration and brain oscillatory activities is still unknown. Yet such information is crucial for a comprehensive understanding of how the different components of fear response collectively modulate rat's brain neural dynamics. Here we trained male rats in an odor fear conditioning task, while recording simultaneously local field potentials in BLA, mPFC and olfactory piriform cortex, together with USV calls and respiration. We show that USV calls coincide with an increase in delta and gamma power and a decrease in theta power. In addition, during USV emission in contrast to silent freezing, there is no coupling between respiratory rate and delta frequency, and the modulation of fast oscillations amplitude relative to the phase of respiration is modified. We propose that sequences of USV calls could result in a differential gating of information within the network of structures sustaining fear behavior, thus potentially modulating fear expression/memory.

Significance Statement

While freezing is the most frequently used measure of fear, it is only one amongst the different components of rodents' response to threatening events. USV is another index that gives additional insight into the socioemotional status of an individual. Our study is the first to describe the effects of USV production on rat's brain oscillatory activities in the fear neural network, and to relate some of them to changes in nasal breathing. A better knowledge of the impact of social vocalizations on brain neural dynamics is not only important for understanding the respective weight of the different components of fear response, but is also particularly relevant for rodent models of human neuropsychiatric disorders, for which socio-affective communication is severely impaired.

Introduction

Fear behavior has been shown to depend on the interaction between the median prefrontal cortex (mPFC) and the basolateral amygdala (BLA), and to involve synchronized activity in theta (4–12 Hz) and gamma (30–120 Hz) frequency oscillations (Seidenbecher et al, 2003; Popa et al, 2010; Headley and Paré, 2013; Herry and Johansen, 2014; Likhtik et al, 2014; Stujenske et al, 2014; Bocchio et al, 2017). In addition, recent studies have shown that freezing, the most used index of fear response in rodents, temporally coincides with the development of sustained 4-Hz oscillations causally involved in the synchronization of spiking activity between prelimbic mPFC and amygdala (Dejean et al, 2016; Karalis et al, 2016). Importantly, this slow oscillation is distinct from the theta rhythm and predicts the onset and offset of freezing. Interestingly, recent work has shown that freezing-related 4Hz oscillation in the prelimbic mPFC was correlated with the animal's respiratory rate, and that disruption of olfactory inputs to the mPFC significantly reduces the 4-Hz oscillation in this structure (Moberly et al, 2018). These data bring further support to the growing body of evidence showing that in addition to its impact on olfactory regions (for a review see Buonviso et al, 2006), nasal respiration also entrains oscillations in widespread brain regions including those involved in the fear network like the mPFC and amygdala (for a review see Tort et al, 2018). This suggests that the breathing rhythm, akin to slow oscillatory rhythms, could help coordinate neural activity across distant brain regions (Jensen and Colgin, 2007; Heck et al, 2017), and potentially modulate emotional/cognitive processes.

Freezing is only one amongst the different components of rodents' response to a threatening event. In aversive situations, such as exposure to predator or footshock, rats also emit 22-kHz ultrasonic vocalizations (USV) (Schwarting and Wöhr, 2012). They indicate a negative emotional state and are associated with the termination of social behavior and the

avoidance of social contacts. Their study provides a powerful tool to assess emotionality and social behavior in animal models of pathologies like autism (Wöhr and Scattoni, 2013). Surprisingly, to our knowledge no study has assessed the impact of USV production on the animal's brain neural dynamics. Yet such information is crucial to understand how the different components of fear response collectively modulate rat's brain neural dynamics. Indeed the emission of USV is considered as reflecting a change in emotional level and 22-kHz USV rates increase with the aversiveness of the situation, as evidenced when foot shock intensity is increased (Wöhr et al. 2005; Hegoburu et al, 2011). Importantly, 22-kHz USV emission drastically slows down the animal's respiratory rate (Frysztak and Neafsey, 1991; Hegoburu et al, 2011; Sirotin et al, 2014; Boulanger-Bertolus et al, 2017), potentially disrupting the respiratory-related brain rhythm described above. The present study thus aimed 1) to investigate whether USV emission coincides with specific changes in oscillatory activities in the fear neural network, and 2) to assess to what extent these changes are related to changes in respiratory rate.

To do so, rats were trained in an odor fear conditioning paradigm while local field potentials (LFP) in BLA, mPFC and olfactory piriform cortex (PIR) were monitored simultaneously with USV calls, behavior and respiration, during the post-shock period. BLA and mPFC were chosen for their well-known role in learned fear acquisition and expression (Corcoran and Quirk, 2007; LeDoux, 2000). The PIR was included as a recording site because it is involved in odor fear conditioning (Sevelinges et al, 2004; Hegoburu et al, 2009, 2014; Sacco and Sacchetti, 2010) and establishes direct connections with both the PFC (Clugnet and Price, 1987) and the amygdala (McDonald, 1998). We report that USV emission temporally coincides with a significant increase in delta, beta and gamma activities while a decrease in theta activity is observed. In addition, we show that some of these changes co-occur with

120 USV-induced changes in respiration. The present data suggest that USV calls could result in a
121 differential gating of information within the fear neural network, thus potentially modulating
122 fear memory/expression.
123

124 ## Material and Methods

125 ***Animals***

126 Data were obtained from twenty-two male Long Evans rats (250-270g at their arrival, Janvier
127 Labs, France). They were housed individually at 23◦C and maintained under a 12 h light–dark
128 cycle (lights on from 8:00 am to 8:00 pm). Food and water were available ad libitum. All
129 experiments and surgical procedures were conducted in strict accordance with the European
130 Community Council Directive of 22nd September 2010 (2010/63/UE) and the national ethics
131 committee (APAFIS#10606). Care was taken at all stages to minimize stress and discomfort
132 to the animals.
133

134 ***Surgery***

135 Animals were anesthetized with Equithesin, a mixture of chloral hydrate (127 mg/kg, i.p.)
136 and sodium pentobarbital (30 mg/kg, i.p.), and placed in a stereotaxic frame (Narishige,
137 Japan) in a flat skull position. The level of anesthesia was held constant with regular
138 injections of Equithesin throughout the experiment. Monopolar stainless steel recording
139 electrodes (100 µm in diameter) were then stereotaxically implanted in the left hemisphere
140 in the three brain areas: PIR (AP: -1.8, L: +5.5mm, DV: -8 mm), mPFC (AP: +3.0mm; L:
141 +0.8mm; DV: -3.5mm) and BLA (AP : -2.8mm, L : +4.9mm, DV : -7.5mm). Accurate positioning
142 in the PIR was achieved using the characteristic profiles of evoked field potential induced in
143 the PIR in response to electrical stimulation of the olfactory bulb (Haberly, 1973). For this, a

144 bipolar stimulation electrode (made of two 100-µm stainless-steel wires with a tip
145 separation of 500 µm) was lowered transiently in the olfactory bulb to facilitate positioning
146 in the PIR and withdrawn thereafter. A reference electrode was screwed in the skull above
147 the right parietal lobe. The three recording electrodes were connected to a telemetry
148 transmitter (rodentPACK system, EMKA Technologies, Paris, France) fixed to the rat's skull
149 surface by dental acrylic cement and anchored with a surgical screw placed in the frontal
150 bone. The animals were allowed to recover for two weeks following surgery.
151
152 ***Experimental apparatus***
153 The apparatus has been described in detail in a previous study (Hegoburu et al., 2011). It
154 consisted of a whole body customized plethysmograph (diameter 20 cm, height 30 cm, Emka
155 Technologies, France) placed in a sound-attenuating cage (L 60 cm, W 60 cm, H 70 cm, 56dB
156 background noise). The plethysmograph was used to measure respiratory parameters in
157 behaving animals. The ceiling of the plethysmograph was equipped with a tower allowing
158 the introduction of a condenser ultrasound microphone (Avisoft-Bioacoustics CM16/CMPA,
159 Berlin, Germany) to monitor USV emitted by the rats. The bottom of the animal chamber
160 was equipped with a shock floor connected to a programmable Coulbourn shocker (Bilaney
161 Consultants GmbH, Düsseldorf, Germany). Three Tygon tubing connected to a
162 programmable custom olfactometer were inserted in the tower on the top of the
163 plethysmograph to deliver air and odorants. Deodorized air flowed constantly through the
164 cage (2 L/min). When programmed, an odor (McCormick Pure Peppermint; 2 L/min; 1:10
165 peppermint vapor to air) was introduced smoothly in the air stream through the switching of
166 a solenoid valve (Fluid automation systems, CH-1290 Versoix, Switzerland) thus minimizing
167 its effect on change in pressure. The bottom of the animal chamber had a port connected to

168 a ventilation pump which could draw air out of the plethysmograph (at a rate of up to 2
169 L/min) thus maintaining a constant airflow that did not interact with the animal's breathing
170 pattern. Animal's behavior was monitored with two video cameras on the walls of the
171 sound-attenuating cage.
172
173 ***Fear conditioning paradigm and data acquisition***
174 After the recovery period, the animals were handled individually and placed in the
175 experimental apparatus for 30 min each day during 3 to 4 days before the beginning of the
176 experiments in order to familiarize them with being manipulated and connected to the
177 telemetry transmitter.
178 For the conditioning session, the telemetry transmitter was plugged on the animal's head
179 and the rat was allowed free exploration during the first 4 min, then an odor was introduced
180 into the cage for 20 or 30s sec, the last second of which overlapped with the delivery of a
181 0.4mA foot-shock. The animal received 10 odor-shock trials, with an intertrial interval of 4
182 min. After the last pairing, the transmitter was unplugged and the animal returned to its
183 home cage.
184
185 ***Retention test***
186 The conditioned fear response was assessed during a retention test carried out 48h after
187 conditioning. For the retention test, the rat was placed in the experimental cage (equipped
188 with new visual cues and with a plastic floor to avoid contextual fear expression) and
189 allowed a 4-min odor-free period. The CS odor was then presented five times for 20s with a
190 4-min intertrial interval. The animal's freezing response was quantified during each 20s-odor
191 presentation and averaged across the 5 trials.

Data acquisition and preprocessing

For USV recording, *t*he ultrasound microphone was connected to a recording interface (UltraSoundGate 116 Hb, Avisoft-Bioacoustics) with the following settings: sampling rate = 214285 Hz; format = 16 bit (Wohr et al., 2005). Recordings were transferred to Avisoft SASLab Pro (version 4.2, Avisoft Bioacoustics, Berlin, Germany) and a Fast Fourier Transform (FFT) was conducted. Spectrograms were generated with an FFT-length of 512 points and a time window overlap of 87.5% (100% Frame, FlatTop window). These parameters produced a spectrogram at a frequency resolution of 419 Hz and a time resolution of 0.29 ms. The acoustic signal detection was provided by an automatic whistle tracking algorithm with a threshold of −20 dB, a minimum duration of 0.01 s and a hold time of 0.02 s. However, the accuracy of detection was verified trial by trial by an experienced user. The main parameters used in the present study were extracted using Avisoft SASLab Pro and concerned the duration as well as the peak amplitude and peak frequency of USV calls. No band pass filter has been applied during USV recording. Although a few 50-kHz USV were observed following shock delivery, in the present study we focused on 22-kHz USV.

The respiratory signal collected from the plethysmograph was amplified and sent to an acquisition card (MC-1608FS, Measurement Computing, USA; Sampling rate = 1000 Hz) for storage and offline analysis. The detection of the respiratory cycles was achieved using an algorithm described in a previous study (Roux et al., 2006). This algorithm performs two main operations: signal smoothing for noise reduction, and detection of zero-crossing points to define accurately the inspiration and expiration phase starting points. Momentary

215 respiratory frequency was determined as the inverse of the respiratory cycle (inspiration
216 plus expiration) duration.
217 The video signals collected through the two cameras were transmitted to a video acquisition
218 card and a homemade acquisition software. Offline, freezing behavior defined as the
219 absence of any visible movement except that due to breathing (Blanchard and Blanchard,
220 1969), was automatically detected using a Labview homemade software and further verified
221 by an experimenter. For this, on each video recording, two successive images were
222 subtracted and the resulting image was binarized using a grey level threshold. The pixels
223 below this threshold were encoded in black and those above the threshold in white. The
224 absence of white pixels on the image resulted in the scoring of Freezing state. Then the same
225 analysis was carried out for the next images of the video recording. The animal's freezing
226 behavior was thus analyzed with a 40ms (two consecutive images) time bin. As a final step,
227 in accordance with classical encoding of freezing behavior in the literature, only freezing
228 episodes lasting longer than 1s were considered as stable freezing behavior. Behaviors other
229 than freezing were manually checked and classified. Escape attempts was scored when the
230 animal exhibited wall climbing, running or saccadic head movements. Although the latter do
231 not involve directed locomotion due to the small size of the plethysmograph, they are clearly
232 different from active exploratory behavior. They might have been induced by the small size
233 of our cage and the absence of any escape route.
234 Local field potentials (LFP) were collected by telemetry via a three-channel wireless
235 miniature transmitter (<5.2g, RodentPack EMKA Technology). LFP signals were amplified
236 (x1000), filtered (between 0.1 and 100 Hz), digitized (sampling frequency: 1000 Hz) and
237 stored on a computer for offline analysis.
238

239 ***Data analysis***

240 *Data selection and experimental categories*

241 Since the aim of the study was to assess the relationship between USV emission, respiration
242 and brain oscillatory activity, we focused our analysis on the 1-min period following shock
243 delivery during which USV were numerous and loud. During this period, the animal's
244 behavior was of two types: Freezing or Escape attempt. No other type of behavior (like
245 grooming, exploration, quiet immobility…) was observed. We first noticed that while the
246 majority of USV were emitted during freezing, a substantial amount of USV also occurred
247 during Escape behavior. This led us to distinguish four types of experimental categories:
248 Silent Freezing, USV Freezing, Silent Escape and USV Escape (Figure 1). For each category,
249 only segments longer than 1s were considered for further analysis.

250 *LFP signals Spectral analysis*

251 The different data (respiration, USV, behavior, LFP signals) were synchronized offline via a
252 TTL synchronization signal generated at the beginning of each experimental session. Once
253 synchronized, the data were analyzed using custom-written scripts under Python.

254 The LFP signals were first individually inspected in order to eliminate artifacts due to signal
255 saturation or transient signal loss. The selection was made for each recording site separately
256 and proceeded as follows: when the duration of an artifact exceeded 5s over the 60s post-
257 shock recording, the trial was excluded. When the number of excluded trials exceeded 5 (out
258 of the 10 trials) then the recording site was excluded for this animal. This procedure led to
259 the following number of animals per recording site for all the electrophysiological data : BLA,
260 n=14; CPF, n=21; PIR, n=20. Because the average duration of individual USV calls was too
261 short to allow proper oscillatory activity analysis (notably for the slow oscillations), we
262 carried out the analysis on blocks of USV corresponding to successive USV with less than 1s

between each other (Figure 1). As soon as the interval between two USV exceeded 1s, then a new block was defined. The periods between USV blocks are considered as Silent periods.

The power spectral density (PSD) of the LFP signals was calculated using the continuous Morlet wavelet transform (Kronland-Martinet et al., 1987) instead of the classical windowed Fourier transform. Indeed the continuous wavelet transform is less susceptible to non-stationary events and offers a better time–frequency resolution. The Morlet wavelet estimated the amplitude of the signal at each time and frequency bin. The obtained time frequency map was then segmented in periods of interest with variable durations (corresponding to the four above defined experimental categories) and averaged per category. Four frequency bands were identified for the subsequent analyses: delta (0-5Hz), theta (5-15Hz), beta (15-40Hz) and gamma (40-80Hz) and the mean power in the different frequency bands was calculated. The values obtained for each recording site were averaged across animals.

Covariation of LFP slow (delta and theta) oscillatory frequency and respiratory frequency

To study frequency-frequency coupling between LFP signals and respiration, we did not use classical coherence analysis because the respiratory signal is not always sinusoidal (especially during USV calls, see Figure 5A). We therefore designed a homemade method allowing to track instantaneous frequency synchrony. To do so, for each detected respiratory cycle, the frequency was estimated as 1/cycle duration and the time course of the instantaneous respiratory frequency was extracted. In parallel, the continuous Morlet scalogram for the LFP signal was computed in our frequency band of interest (0-15Hz). At each time bin (4ms), the local maximum in the instantaneous power spectrum was extracted together with the corresponding instantaneous frequency of the LFP signal. The time course of the predominant instantaneous frequency curve of the LFP was then extracted. From the two

287 times series obtained (instantaneous respiration frequency and predominant instantaneous
288 LFP frequency), a 2D matrix histogram was built, with the respiratory frequency represented
289 on the X-axis and the LFP frequency on Y-axis. This 2D histogram was normalized so that the
290 total sum is 1, and point density was represented on a color scale ranging from blue to
291 yellow as the point density increases. The existence of a coupling between respiration
292 frequency and LFP frequency can be assumed when a high point density (ie yellow color) is
293 observed along the diagonal of the 2D histogram (see Figure 6 for an illustration).
294 Conversely, in the absence of coupling a non-correlated gaussian shape is observed. The two
295 possibilities can co-occur on the same 2D histogram.

296 *Modulation of LFP beta and gamma power by respiratory cycle phase*

297 To investigate whether LFP beta and gamma amplitudes were modulated by respiration
298 phase, we computed a so called "cycle-frequency scalogram" of the LFP signal (adapted from
299 Roux et al, 2007). In analogy to a classical time-frequency map that computes the energy of
300 LFP signal over time and frequency, we computed the energy of LFP signal over respiratory
301 cycle duration and frequency. Briefly this method consists in three steps 1) Compute the
302 continuous Morlet scalogram (time-frequency map) 2) Use detected respiratory cycle to
303 segment this scalogram in 2 phases (inhalation, exhalation) 3) Stretch by linear interpolation
304 each segment so that all the segments fit the same normalized template (range from 0 to 1,
305 with a 0.025 bin). The result of this analysis is very similar to the classical time frequency
306 scalogram except that it presents small time distortions locally that do not affect the
307 instantaneous power. Since all the cycles were normalized to the same size, they were
308 averaged together. The typical template of an individual respiratory cycle is defined as
309 follows: inhalation from 0 to 0.4 and exhalation from 0.4 to 1. This ratio corresponds to the
310 average value calculated over all cycles and animals. On the scalogram, LFP signal power for

311 the different frequency bands is represented using a color scale ranging from blue to yellow
312 as the power increases (see Figure 7B for an illustration). The maximum power in the beta
313 and gamma bands was also extracted and represented on a curve throughout the
314 respiratory cycle.
315
316 ***Statistical analysis***
317 All analyses were performed with Systat 13.0® software. For each test, the significance level
318 was set at $p<0.05$.
319 USV parameters (Figure 2; Duration, peak amplitude, peak frequency) were compared
320 between USV Freezing and USV Escape using paired t-tests.
321 Average LFP oscillatory activity parameters (Figure 3, 4; power, peak amplitude, frequency)
322 are calculated in the different frequency bands: delta (0–5 Hz), theta (5-15 Hz), beta (15-40
323 Hz) and gamma (40-80 Hz), and expressed as means ± SEM across animals. A three-way
324 (Structure, USV and Behavior) ANOVA for repeated measures was first applied to assess
325 between structures differences in the four experimental categories defined above. Then, for
326 each structures, a two-way (USV and Behavior) ANOVA for repeated measures was applied
327 followed by post-hoc multiple comparisons.
328 The time course of beta and gamma activity power throughout the respiratory cycle (Figures
329 8 and 9) was first compared using a three-way ANOVA (Behavior, USV and Respiratory cycle
330 time), followed by a two-way ANOVA for repeated measures (USV and Respiratory cycle
331 time) carried out separately for Freezing and Escape condition.

Histology

At the end of the experiment, the animals were killed with a lethal dose of pentobarbital, their brains were removed, postfixed, cryoprotected in sucrose (20%). The brains were then sectioned (40µm coronal slices) for verification of electrodes tips by light microscopy. Areas targeted by the electrodes in the three implanted brain regions have been reported on brain atlas coronal sections (Figure 1-1).

Results

22-kHz USV are observed during both passive and active defense responses

The 1-min period following shock delivery was analyzed for behavior, USV emission and brain oscillatory activity. During this period, the animal's behavior was of two types: Freezing or Escape attempts. While the majority of USV were emitted during freezing, a non-negligible amount of USV also occurred during Escape. Figure 2A illustrates the repartition of the four categories throughout the 1-min post-shock period. The animals spent 70.3% of the time in Freezing vs 29.7% in Escape. While the animals spent similar amounts of time in Silent Freezing compared to USV Freezing, they spent more time in Silent Escape than in USV Escape. Figure 2B reports the mean behavior duration in the four conditions and the mean USV rate during the 1-min post-shock period.

We then compared the characteristics of the USV emitted during Freezing versus Escape. Paired t-test comparisons revealed that call duration (Figure 2C) was significantly lower for USV emitted during Escape than during Freezing (t_{21} = 2.198, p-value = 0.039), while call peak amplitude (Figure 2D) and peak frequency (Figure 2E) was significantly higher during

Escape than during Freezing (peak amplitude: t_{21} = -3.957, p-value = 0.001; peak frequency: t_{21} = -3.928, p-value =0.001).

Finally we assessed whether the amount of USV (USV Freezing or USV Escape) emitted during conditioning could predict the animal's performance during the retention test carried out 48h later (Figure 2F). We showed that the number of USV Freezing was positively correlated with the amount of freezing at retention (Pearson correlation coefficient: R_{22}=0.49, p<0.02) while the number of USV Escape was not (R_{22}=0.19).

In summary, 22-kHz USV are emitted during both passive (Freezing) and active (Escape) defense responses. USV emitted during Escape are shorter and louder than those emitted during Freezing, and exhibit a higher peak frequency. In addition, the amount of USV Freezing during training was a good predictor of the animal's learned fear response at retention.

USV emission is associated with changes in oscillatory activity power

The main objective of this experiment was to assess whether USV emission is associated with changes in oscillatory activity power compared to the silent behavioral state, and if these changes are similar across the three recording sites. Because USV are emitted during two different defense responses, we also compared oscillatory activity power between these two behavioral states (Freezing versus Escape).

Delta (0-5Hz) and theta (5-15Hz) bands mean power spectral density

For each recording site, LFP mean power spectral density was calculated per animal and averaged across animals (Figure 3, left part). It can be observed that in each recording site, the signal power in the delta and theta bands depends both on the animal's behavioral state

379 (Freezing vs Escape) and for a given behavioral state, on the emission of USV (USV vs Silent).
380 Averaged mean power was calculated for each frequency band, in the four categories.

381 ***Delta band mean power*** (Figure 3, middle column)

382 A three-way ANOVA revealed no main effect of Structure ($F_{2,52}$=1.38, p=0.3), but a significant
383 USVxBehaviorxStructure interaction ($F_{2,52}$=3.23, p=0.05). In each recording sites, a two-way
384 ANOVA revealed a significant main effect of factors USV and Behavior, and no significant
385 USVxBehavior interaction except for the mPFC (see Table 1 for all the statistical results).
386 Post-hoc comparisons first showed that in the three structures, delta mean power was
387 higher during Silent Freezing than during Silent Escape. In addition, in both behavioral states
388 (except for mPFC for which the effect of USV was only significant during Escape), the
389 emission of USV was associated with a significant enhancement in delta mean power.

390 ***Theta band mean power*** (Figure 3, right column)

391 The three-way ANOVA revealed no main effect of Structure ($F_{2,52}$=0.38, p=0.7), but a
392 significant USVxStructure interaction ($F_{2,52}$=4.72, p=0.01). In BLA and mPFC, the two-way
393 ANOVA revealed a significant main effect of factors USV and Behavior, and no significant
394 USVxBehavior interaction (see Table 1, upper part). In PIR, no significant effect of factor USV
395 was observed. Post-hoc comparisons (see Table 1, lower part) showed that in the three
396 structures, theta mean power was lower during Silent Freezing than during Silent Escape.
397 Moreover, in BLA and mPFC, USV emission was associated with a decrease in theta mean
398 power.

399

400 In summary, when compared to Silent Escape, Silent Freezing is characterized by a higher
401 power of oscillatory activity in the delta band while a lower power was observed in the theta
402 band. Importantly, in both Freezing and Escape states, the emission of USV coincides globally

with an increase in power in the delta band in all three regions and a decrease in the theta band in BLA and mPFC.

Beta (15-40Hz) and gamma (40-80Hz) bands mean power spectral density

Mean power spectral density of local field potentials is represented for each recording site on Figure 4, left part.

that in each recording site, the signal power in the gamma band depends on both the animal's behavioral state (Freezing vs Escape) and, for a given behavioral state, the emission of USV (USV vs Silent). Furthermore, in the PIR, the signal power in the beta band also seems to be affected during the emission of USV during Escape. Averaged mean power was calculated for each frequency band, in the four categories.

Beta band mean power (Table 2)**:**

Beta band mean power values in the three recording sites are reported on Table 2 (upper part). The three-way ANOVA revealed a significant main effect of Structure ($F_{2,52}$=4.24, p=0.02), and a significant interaction for USVxStructure ($F_{2,52}$=4.10, p=0.02), BehaviorxStructure ($F_{2,52}$=5.15, p=0.009) and USVxBehaviorxStructure ($F_{2,52}$=5.32, p=0.008). The two-way ANOVA revealed no significant changes in beta activity in the BLA (Table 2, middle part). In the mPFC, a significant main effect of USV was observed, and post-hoc comparisons showed that USV emission during both Escape and Freezing induced an increase in beta mean power (Table 2, lower part). In the PIR, a significant main effect of USV and Behavior, and a significant USVxBehavior interaction were observed. Post-hoc comparisons showed that USV emission during Escape was associated with an increase in beta mean power.

Gamma band mean power (Figure 4, right column)**:**

427 The three-way ANOVA revealed a significant main effect of Structure ($F_{2,52}$=3.69, p=0.02),
428 and a significant interaction for USVxStructure ($F_{2,52}$=4.20, p=0.02) and BehaviorxStructure
429 ($F_{2,52}$=5.29, p=0.008). The two-way ANOVA revealed a significant main effect of Behavior,
430 and a significant USVxBehavior interaction in the three recording sites (Table 3). Post-hoc
431 comparisons showed that gamma mean power was lower during Silent Freezing than during
432 Silent Escape. In addition, USV emission during Escape temporally coincided with an increase
433 in gamma mean power. Noteworthy, USV emission during both Freezing and Escape was
434 associated with a narrowing of the activity towards the lower range of the band and an
435 increase in gamma peak power (as can be seen on the power spectra of Figure 4, left
436 column).
437
438 In summary, during Silent Freezing, gamma band mean power is lower than during Silent
439 Escape. In addition, the emission of USV coincides with an increase in gamma band activity
440 (mainly during escape) added to a narrowing of the activity towards the lower range of the
441 band where the peak power is increased. Finally, in the PIR and mPFC (but not in BLA), the
442 emission of USV during Escape is associated with an increase in beta activity power.
443
444 **USV emission strongly affects instantaneous respiratory rate**
445 As previously reported in the literature, we found that the emission of USV drastically
446 changes the shape and frequency of the respiratory signal (see individual examples on Figure
447 5A). Figure 5B illustrates the PDF of respiration in our four experimental categories. A three-
448 way ANOVA revealed a highly significant BehaviorxUSVxRespiratory Frequency interaction
449 ($F_{32,1344}$=5.44, p<0.000001) and further two-way ANOVAs showed a significant main effect of
450 USV for both Freezing ($F_{1,21}$=6.29, p=0.02) and Escape ($F_{1,21}$=18.05, p=0.0004) states. The

emission of USV shifts the dominant respiratory frequency toward lower values, going from 6.3Hz to 1.4Hz for Escape and from 2.8Hz to 1Hz for Freezing (Figure 5B, insert). The next step of our study was then to assess to what extent the frequency of oscillatory activity in the delta and theta range followed respiratory frequency, and consequently whether USV emission has an impact on this relationship.

Covariation between delta and theta oscillatory frequencies and respiratory frequency

Figure 6 (upper part) highlights the fact that the respiratory frequency range delimits the range of LFP oscillatory frequency for which co-variation between the two signals frequency could be assessed.

In each experimental category, we carried out covariation matrices (Figure 6, lower part) depicting pairwise similarities between respiratory frequency and oscillatory frequency in the delta and theta bands. During Silent Escape and USV Escape, theta activity is preferentially expressed and shows no obvious coupling with respiration: whatever the respiratory frequency, theta activity is mostly observed with a fixed frequency around 6-7Hz. During Silent Freezing, both theta and delta activities are expressed. While a clear-cut covariation is observed between delta frequency and respiratory frequency, no covariation is seen for theta frequency. During USV Freezing, both theta and delta activities are expressed with no coupling with respiratory frequency. Raw signal traces recorded in the same animal in the four experimental categories are reported on Figure 6-1.

In summary, the only experimental category leading to a clear-cut frequency-frequency coupling between respiration and LFP signal is Silent Freezing and concerns the delta band. During USV emission, no covariation is observed between respiratory rate and delta or theta oscillatory activities.

Modulation of beta and gamma power with the phase of the respiratory cycle

It was shown that respiration can modulate not only slow neuronal oscillations, but also beta and gamma band oscillations, which amplitude is modulated in phase with respiration (Cenier et al, 2009; Ito et al., 2014). We therefore investigated whether activity in the beta and gamma bands was modulated by the phase of the respiratory cycle in our different experimental categories, and whether USV emission has an impact on this modulation. Figure 7A illustrates an individual example of LFP signal collected in the PIR, with the corresponding respiratory signal and USV calls. A time frequency analysis carried out on the LFP signal at the level of the respiratory cycle, clearly shows that respiration modulates beta and gamma activity power, with higher beta activity power at the beginning of expiration and higher gamma activity throughout expiration. This modulation is further evidenced by the analysis illustrated on Figure 7B which represents the respiration phase-frequency map of LFP signal in the four experimental categories. We carried out this analysis in the three recording sites (Figure 7-1). The data illustrated on Figure 8 represent the time course of beta activity maximal power throughout the respiratory cycle. A three-way (Behavior, Respiratory cycle time, USV) ANOVA first revealed a significant main effect of Behavior in mPFC ($F_{1,40}$=6.38, p=0.02) and PIR ($F_{1,38}$=7.93, p=0.008), and a significant Respiratory cycle timexBehavior interaction in BLA ($F_{39,1014}$=2.47, $p=2x10^{-6}$). We then analyzed the data separately for Freezing and Escape to compare the time course of LFP oscillatory activity power throughout the respiratory cycle, either with or without USV. During Freezing (Figure 8, left part), a two-way ANOVA revealed a significant effect of Respiratory cycle time in the three recording sites and a significant interaction for USVxRespiratory cycle time in the PIR only (see Table 4, upper part). In this recording site, during Silent Freezing, the maximum

power is observed during inspiration, while during USV Freezing, the maximum is shifted toward the early part of expiration. Concerning Escape (Figure 8, right part), in the three recording sites the ANOVA revealed a significant effect of Respiratory cycle time but no effect of USV or USVxRespiratory cycle interaction (see Table 4, upper part). The time course of gamma activity maximal power throughout the respiratory cycle is reported on Figure 9. The three-way (Behavior, Respiratory cycle time, USV) ANOVA revealed a significant Respiratory cycle timexUSVxBehavior interaction in BLA ($F_{39,1014}$=0.58, p=1x10^{-7}), mPFC ($F_{39,1560}$=3.75, p=1x10^{-7}) and PIR ($F_{39,1482}$=4.18, p=1x10^{-7}). We then analyzed the data separately for Freezing and Escape. During Freezing (Figure 9, left part), the two-way ANOVA revealed a significant effect of Respiratory cycle time and a significant interaction for USVxRespiratory cycle time in the three recording sites (see Table 4, lower part). During Silent Freezing, the maximum power is observed during inspiration, while during USV Freezing, two maxima are observed, one during inspiration, and the other during the late part of expiration. Concerning Escape, (Figure 9, right part), the ANOVA revealed a significant effect of Respiratory cycle time and USV (except for BLA), and a significant interaction for USVxRespiratory cycle (see Table 4, lower part). During Silent Escape, the maximum power is observed at the transition between inspiration and expiration, while during USV Escape, the maximum is shifted toward inspiration.

In summary, in the PIR beta power is modulated by the phase of the respiratory cycle during Freezing and the pattern of this modulation is changed during USV emission. Gamma power in the three recording sites is strongly modulated by the phase of the respiratory cycle during both Freezing and Escape, although presenting slightly different patterns. The emission of USV is associated with drastic changes in the time course of this modulation.

Discussion

The present study assessed for the first time the impact of 22-kHz USV production on brain dynamics in the network involved in fear expression, including the mPFC and the BLA. We report that USV emission modulates oscillatory activities differentially depending on their frequency band. Specifically, it temporally coincides with an increase in delta and gamma power, and a decrease in theta power. In addition, in the PIR, an increase in beta activity is observed. Some of these changes co-occur with USV-induced respiration changes. Indeed, during USV calls, the coupling observed between respiratory frequency and delta oscillatory frequency during Silent Freezing is lost, and the time course of gamma and beta power within the respiratory cycle is modified. The present data suggest that USV calls could result in a specific gating of information within the fear network, potentially modulating fear memory, as suggested by our observation that the amount of USV emitted during conditioning is a good predictor of the learned fear response at retention.

22-kHz USV are observed during both passive and active fear responses

22-kHz USV in rats are emitted in aversive situations such as foot-shock delivery and are considered as reflecting a negative affective state (Litvin et al, 2007; Schwarting and Wöhr, 2012; Brudzynski, 2013). We found that USV are predominantly produced during Freezing, which is consistent with the literature (Brudzynski and Ocepia, 1992; Wöhr et al, 2005; Hegoburu et al, 2011; Boulanger-Bertolus et al, 2017). However, we also found that some USV are emitted during escape. Although some examples of 22-kHz USV during locomotion have been reported (Laplagne and Elias Costa, 2016; Boulanger-Bertolus et al, 2017), the characteristics of these USV remain poorly investigated. Here we show that 22-kHz USV

emitted during escape are shorter and louder than those emitted during Freezing and exhibit a higher peak frequency.

We also show that although these two types of USV have globally similar effects on brain oscillations, they present different relationships with performance at 48h-retention. Indeed while there is a positive correlation between the number of USV Freezing during conditioning and the amount of Freezing at retention, this correlation is not found for USV Escape. This suggests that the two subtypes of 22-KHz USV reflect different aspects of fear response. For instance, USV Escape might be more related to the unconditioned response to shock, while USV Freezing are generally considered as part of the conditioned fear response (Wöhr and Schwarting, 2008).

Freezing and Escape differentially modulate brain oscillatory activities

We first investigated whether in the absence of USV emission, the way fear is expressed is associated with different changes in brain oscillatory activities. Freezing is a passive defense response while escape is an active response. Recent studies pinpointed that active and passive fear responses involve distinct and mutually inhibitory neurons in the central amygdala (Gozzi et al, 2010; Fadok et al, 2017). Here we show that these two response modes also differentially modulate oscillatory activity in the fear circuit. Indeed, compared to escape, freezing is characterized by a higher delta power and a lower theta and gamma power. Our data in the delta band are in line with the literature as several recent studies showed that freezing temporally coincides with the development of 4-Hz oscillations in prefrontal-amygdala circuits (Dejean et al, 2016; Karalis et al, 2016; Moberly et al, 2018). In awake animals, theta activity is known to occur preferentially during voluntary locomotor activities (Vanderwolf, 1969; Buszaki, 2002), thus explaining the increase in theta power

observed here during escape. Finally, the increase in gamma power observed during escape might reflect an increased emotional level compared to freezing. Indeed, previous studies both in humans and animals have shown that gamma oscillations are enhanced during emotional situations (reviewed in Headley and Paré, 2013; Stujenske et al, 2014; Concina et al, 2018).

22-kHz USV emission alters respiration and is associated with changes in oscillatory activities

While several studies have investigated the neural circuit involved in USV production (reviewed in Schwarting and Wöhr, 2012), and the correlates of USV perception in the brain of conspecifics receivers (Sadananda et al, 2008; Parsana et al, 2012; Roberts and Portfors, 2015), to our knowledge no study has assessed the effect of USV production on the sender animal's brain oscillatory activities. We showed that USV emission coincides with an increase in delta power and a decrease in theta power. In addition, an increase in gamma power is observed. The effects are globally similar for both types of USV, and in the three recording sites although small differences exist. Furthermore, a strong increase in beta power is more specifically observed in the PIR.

Importantly, some of the changes observed during USV emission co-occurred with changes in respiratory rhythm. USV are produced during expiration upon constriction of the vocal folds resulting in an increase in subglottal pressure and a reduction of airflow through the nose (Riede, 2011; Sirotin et al, 2014). Consequently, 22-kHz USV emission induces drastic changes in the shape and frequency of the respiratory signal (Frysztak and Neafsey, 1991; Hegoburu et al, 2011; Boulanger-Bertolus et al, 2017). It is known from a long time that respiration drives oscillations time-locked to breathing cycles in the olfactory pathways

595 (Adrian, 1942; Fontanini and Bower, 2005; Buonviso et al, 2006; Kay et al, 2009; Courtiol et
596 al, 2011; Esclassan et al, 2012; Zelano et al, 2016) and modulates the amplitude of local beta
597 and gamma oscillations in the olfactory bulb (Buonviso et al., 2003; Cenier et al, 2009;
598 Rosero and Aylwin, 2011) and in the olfactory cortex (Fontanini and Bower, 2005; Zelano et
599 al, 2016). Several recent papers have highlighted that outside its impact on olfactory regions,
600 nasal respiration also entrains oscillations in widespread brain regions in awake rodents (Ito
601 et al, 2014; Nguyen Chi et al, 2016; Biskamp et al, 2017; Zhong et al, 2017; Rojas-Líbano et al,
602 2018; Tort et al, 2018) and modulates the amplitude of fast oscillations (Ito et al, 2014;
603 Biskamp et al, 2017; Zhong et al, 2017). Importantly a recent work has specifically
604 investigated the link between respiration and freezing-related 4Hz oscillation in the mPFC
605 (Moberly et al, 2018), and reported that during freezing, mice respiratory frequency is
606 correlated with the 4-Hz oscillation in the mPFC, and that disruption of olfactory inputs to
607 the mPFC significantly reduces the 4-Hz oscillation.
608 Here we show that during Silent Freezing, dominant frequency in the delta band covaries
609 with respiratory frequency. In addition, we report that the activity in the gamma band for
610 the three recording sites, and in the beta band for PIR, are modulated in phase with
611 respiration, with greater beta and gamma power during inspiration than expiration (see
612 summary on Figure 9). Importantly we also show that USV emission, particularly during
613 freezing, coincides with important changes in the relationship between respiration and
614 oscillatory activity. First, USV emission induces a deep slow-down of respiratory frequency.
615 In parallel, the coupling between delta band dominant frequency and respiratory frequency
616 is lost. In addition, a reorganization of beta and gamma activity power during the respiratory
617 cycle occurs, with increased beta power in PIR during the first half of expiration phase, and
618 increased gamma power in the three recording sites during the second half of expiration.

Functional interpretation

How can we integrate the present data to the existing literature? Respiration-locked oscillations in non-olfactory regions were shown to depend on nasal airflow (Ito et al, 2014; Yanovsky et al, 2014). Indeed olfactory sensory neurons have mechanosensitive properties (Grosmaitre et al, 2007) and the signals elicited by rhythmic airflow in the nose are transmitted to the olfactory bulb and the PIR (Fontanini et al, 2003; Wu et al, 2017). The PIR has direct connections with the PFC (Clugnet and Price, 1987) and the olfactory information has unique direct access to the amygdala (McDonald, 1998). We propose that the deep slow-down of respiratory rate added to the reduction of airflow through the nose during USV calls (Riede, 2011; Sirotin et al, 2014) is responsible for the loss of coupling between nasal rhythm and delta oscillation. During USV calls, brain delta oscillations become independent of nasal respiration and their power increases. In parallel, beta and gamma activity power increases during expiration. Interestingly, Manabe and Mori (2013) reported that in olfactory regions, gamma oscillations can lock to different phases of the respiratory cycle depending on the animal's behavior. Indeed, during active exploration with high sniffing rate, gamma is phase-locked to inhalation, while during awake resting in which rats show a slow respiration rate with long exhalation phase, gamma is phase-locked to exhalation. The authors propose that gamma oscillatory coupling can be generated either by olfactory sensory inputs during inhalation, or centrally in the brain during exhalation. The same kind of interpretation could hold for our data, with the emission of USV being associated with a reorganization of gamma coupling during expiration, potentially resulting in a different gating of information to downstream structures of the fear network. Since we observed that the amount of USV emitted during freezing at training is correlated with the learned freezing response at

643 retention, we suggest that the window of a USV call and its particular respiratory pattern
644 added to its specific combination of brain oscillatory activity, might enhance plasticity at
645 given sites of the network and ultimately strengthen long-term fear memory. Additional
646 experiments are needed to explore the causal link between USV-related changes in
647 oscillatory activities and fear memory.
648 A better knowledge of the impact of USV production on brain neural dynamics is not only
649 important for understanding the respective weight of the different components of fear
650 response, but is also particularly relevant for rodent models of human neuropsychiatric
651 disorders, for which socio-affective communication is severely impaired (Wöhr and Scattoni,
652 2013).

REFERENCES

Adrian ED (1942) Olfactory reactions in the brain of the hedgehog. J Physiol 100:459-473.

Blanchard RJ, Blanchard DC (1969) Crouching as an index of fear. J Comp Physiol Psychol 67:370-375.

Bocchio M, Nabavi S, Capogna M (2017) Synaptic Plasticity, Engrams, and Network Oscillations in Amygdala Circuits for Storage and Retrieval of Emotional Memories. Neuron 94:731-743.

Boulanger Bertolus J, Hegoburu C, Ahers JL, Londen E, Rousselot J, Szyba K, Thevenet M, Sullivan-Wilson TA, Doyere V, Sullivan RM, Mouly AM (2014) Infant rats can learn time intervals before the maturation of the striatum: evidence from odor fear conditioning. Front Behav Neurosci 8:176.

Boulanger-Bertolus J, Rincon-Cortes M, Sullivan RM, Mouly AM (2017) Understanding pup affective state through ethologically significant ultrasonic vocalization frequency. Sci Rep 7:13483.

Brudzynski SM, Ociepa D (1992) Ultrasonic vocalization of laboratory rats in response to handling and touch. Physiol Behav 52:655-660.

Brudzynski SM, Bihari F, Ociepa D, Fu XW (1993) Analysis of 22 kHz ultrasonic vocalization in laboratory rats: long and short calls. Physiol Behav 54:215-221.

Brudzynski SM (2005) Principles of rat communication: quantitative parameters of ultrasonic calls in rats. Behav Genet 35:85-92.

Brudzynski SM (2013) Ethotransmission: communication of emotional states through ultrasonic vocalization in rats. Curr Opin Neurobiol 23:310-317.

Buonviso N, Amat C, Litaudon P, Roux S, Royet JP, Farget V, Sicard G (2003) Rhythm sequence through the olfactory bulb layers during the time window of a respiratory cycle. Eur J Neurosci 17:1811-1819.

Buonviso N, Amat C, Litaudon P (2006) Respiratory modulation of olfactory neurons in the rodent brain. Chem Senses 31:145-154.

Buzsaki G (2002) Theta oscillations in the hippocampus. Neuron 33:325-340.

Carmichael ST, Clugnet MC, Price JL (1994) Central olfactory connections in the macaque monkey. J Comp Neurol 346:403-434.

Cenier T, David F, Litaudon P, Garcia S, Amat C, Buonviso N (2009) Respiration-gated formation of gamma and beta neural assemblies in the mammalian olfactory bulb. Eur J Neurosci 29:921-930.

Clugnet, M-C, Price,JL (1987) Olfactory input to the prefrontal cortex in the rat. Annals of the New York Academy of Sciences 510, 231–235

Concina G, Cambiaghi M, Renna A, Sacchetti B (2018) Coherent Activity between the Prelimbic and Auditory Cortex in the Slow-Gamma Band Underlies Fear Discrimination. J Neurosci 38:8313-8328.

Corcoran KA, Quirk GJ (2007) Activity in prelimbic cortex is necessary for the expression of learned, but not innate, fears. The Journal of neuroscience : the official journal of the Society for Neuroscience 27:840-844.

Courtiol E, Hegoburu C, Litaudon P, Garcia S, Fourcaud-Trocme N, Buonviso N (2011) Individual and synergistic effects of sniffing frequency and flow rate on olfactory bulb activity. J Neurophysiol 106:2813-2824.

Dejean C, Courtin J, Karalis N, Chaudun F, Wurtz H, Bienvenu TC, Herry C (2016) Prefrontal neuronal assemblies temporally control fear behaviour. Nature 535:420-424.

Esclassan F, Courtiol E, Thevenet M, Garcia S, Buonviso N, Litaudon P (2012) Faster, deeper, better: the impact of sniffing modulation on bulbar olfactory processing. PloS one 7:e40927.

Fadok JP, Krabbe S, Markovic M, Courtin J, Xu C, Massi L, Botta P, Bylund K, Muller C, Kovacevic A, Tovote P, Luthi A (2017) A competitive inhibitory circuit for selection of active and passive fear responses. Nature 542:96-100.

Fontanini A, Spano P, Bower JM (2003) Ketamine-xylazine-induced slow (< 1.5 Hz) oscillations in the rat piriform (olfactory) cortex are functionally correlated with respiration. J Neurosci 23:7993-8001.

Fontanini A, Bower JM (2005) Variable coupling between olfactory system activity and respiration in ketamine/xylazine anesthetized rats. J Neurophysiol 93:3573-3581.

Frysztak RJ, Neafsey EJ (1991) The effect of medial frontal cortex lesions on respiration, "freezing," and ultrasonic vocalizations during conditioned emotional responses in rats. Cereb Cortex 1:418-425.

Gozzi A, Jain A, Giovannelli A, Bertollini C, Crestan V, Schwarz AJ, Tsetsenis T, Ragozzino D, Gross CT, Bifone A (2010) A neural switch for active and passive fear. Neuron 67:656-666.

Grosmaitre X, Santarelli LC, Tan J, Luo M, Ma M (2007) Dual functions of mammalian olfactory sensory neurons as odor detectors and mechanical sensors. Nat Neurosci 10:348-354.

Headley DB, Pare D (2013) In sync: gamma oscillations and emotional memory. Front Behav Neurosci 7:170.

Heck DH, McAfee SS, Liu Y, Babajani-Feremi A, Rezaie R, Freeman WJ, Wheless JW, Papanicolaou AC, Ruszinko M, Sokolov Y, Kozma R (2016) Breathing as a Fundamental Rhythm of Brain Function. Front Neural Circuits 10:115.

Haberly LB (1973) Summed potentials evoked in opossum prepyriform cortex. Journal of neurophysiology 36:775-788.

Hegoburu C, Sevelinges Y, Thevenet M, Gervais R, Parrot S, Mouly AM (2009) Differential dynamics of amino acid release in the amygdala and olfactory cortex during odor fear acquisition as revealed with simultaneous high temporal resolution microdialysis. Learning & Memory 16:687-697.

Hegoburu C, Shionoya K, Garcia S, Messaoudi B, Thevenet M, Mouly AM (2011) The RUB Cage: Respiration-Ultrasonic Vocalizations-Behavior Acquisition Setup for Assessing Emotional Memory in Rats. Front Behav Neurosci 5:25.

Hegoburu C, Parrot S, Ferreira G, Mouly AM (2014) Differential involvement of amygdala and cortical NMDA receptors activation upon encoding in odor fear memory. Learning & Memory 21:651-655.

Herry C, Johansen JP (2014) Encoding of fear learning and memory in distributed neuronal circuits. Nat Neurosci 17:1644-1654.

Ito J, Roy S, Liu Y, Cao Y, Fletcher M, Lu L, Boughter JD, Grun S, Heck DH (2014) Whisker barrel cortex delta oscillations and gamma power in the awake mouse are linked to respiration. Nat Commun 5:3572.

Jensen O, Colgin LL (2007) Cross-frequency coupling between neuronal oscillations. Trends Cogn Sci 11:267-269.

Karalis N, Dejean C, Chaudun F, Khoder S, Rozeske RR, Wurtz H, Bagur S, Benchenane K, Sirota A, Courtin J, Herry C (2016) 4-Hz oscillations synchronize prefrontal-amygdala circuits during fear behavior. Nat Neurosci 19:605-612.

Kay LM, Beshel J, Brea J, Martin C, Rojas-Libano D, Kopell N (2009) Olfactory oscillations: the what, how and what for. Trends Neurosci 32:207-214.

Kronland-Martinet R, Morlet J, Grossmann A (1987) Analysis of sound patterns through wavelet transforms. Int J Pattern Recog Art Intel 1:273-302.

Laplagne DA, Elias Costa M (2016) Rats Synchronize Locomotion with Ultrasonic Vocalizations at the Subsecond Time Scale. Front Behav Neurosci 10:184.

LeDoux JE (2000) Emotion circuits in the brain. Annual review of neuroscience 23:155-184.

Likhtik E, Stujenske JM, Topiwala MA, Harris AZ, Gordon JA (2014) Prefrontal entrainment of amygdala activity signals safety in learned fear and innate anxiety. Nat Neurosci 17:106-113.

Litvin Y, Blanchard DC, Blanchard RJ (2007) Rat 22kHz ultrasonic vocalizations as alarm cries. Behav Brain Res 182:166-172.

McDonald AJ (1998) Cortical pathways to the mammalian amygdala. Prog Neurobiol 55:257-332.

Moberly AH, Schreck M, Bhattarai JP, Zweifel LS, Luo W, Ma M (2018) Olfactory inputs modulate respiration-related rhythmic activity in the prefrontal cortex and freezing behavior. Nat Commun 9:1528.

Nguyen Chi V, Muller C, Wolfenstetter T, Yanovsky Y, Draguhn A, Tort AB, Brankack J (2016) Hippocampal Respiration-Driven Rhythm Distinct from Theta Oscillations in Awake Mice. J Neurosci 36:162-177.

Parsana AJ, Li N, Brown TH (2012) Positive and negative ultrasonic social signals elicit opposing firing patterns in rat amygdala. Behav Brain Res 226:77-86.

Paxinos G, Watson C (2007). The rat brain in stereotaxic coordinates. San Diego, CA: AcademicPress.

Popa D, Duvarci S, Popescu AT, Lena C, Pare D (2010) Coherent amygdalocortical theta promotes fear memory consolidation during paradoxical sleep. Proc Natl Acad Sci USA 107:6516-6519.

Riede T (2011) Subglottal pressure, tracheal airflow, and intrinsic laryngeal muscle activity during rat ultrasound vocalization. J Neurophysiol 106:2580-2592.

Roberts PD, Portfors CV (2015) Responses to Social Vocalizations in the Dorsal Cochlear Nucleus of Mice. Front Syst Neurosci 9:172.

Rojas-Libano D, Wimmer Del Solar J, Aguilar-Rivera M, Montefusco-Siegmund R, Maldonado PE (2018) Local cortical activity of distant brain areas can phase-lock to the olfactory bulb's respiratory rhythm in the freely behaving rat. J Neurophysiol 120:960-972.

Rosero MA, Aylwin ML (2011) Sniffing shapes the dynamics of olfactory bulb gamma oscillations in awake behaving rats. Eur J Neurosci 34:787-799.

Roux SG, Cenier T, Garcia S, Litaudon P, Buonviso N (2007) A wavelet-based method for local phase extraction from a multi-frequency oscillatory signal. J Neurosci Methods 160:135-143.

Sacco T, Sacchetti B (2010) Role of secondary sensory cortices in emotional memory storage and retrieval in rats. Science 329:649-656.

Sadananda M, Wohr M, Schwarting RK (2008) Playback of 22-kHz and 50-kHz ultrasonic vocalizations induces differential c-fos expression in rat brain. Neurosci Lett 435:17-23.

Schwarting RK, Wohr M (2012) On the relationships between ultrasonic calling and anxiety-related behavior in rats. Braz J Med Biol Res 45:337-348.

Seidenbecher T, Laxmi TR, Stork O, Pape HC (2003) Amygdalar and hippocampal theta rhythm synchronization during fear memory retrieval. Science 301:846-850.

Sevelinges Y, Gervais R, Messaoudi B, Granjon L, Mouly AM (2004) Olfactory fear conditioning induces field potential potentiation in rat olfactory cortex and amygdala. Learning & memory 11:761-769.

Shionoya K, Hegoburu C, Brown BL, Sullivan RM, Doyere V, Mouly AM (2013) It's time to fear! Interval timing in odor fear conditioning in rats. Front Behav Neurosci 7:128.

Sirotin YB, Costa ME, Laplagne DA (2014) Rodent ultrasonic vocalizations are bound to active sniffing behavior. Front Behav Neurosci 8:399.

Stujenske JM, Likhtik E, Topiwala MA, Gordon JA (2014) Fear and safety engage competing patterns of theta-gamma coupling in the basolateral amygdala. Neuron 83:919-933.

Tort ABL, Brankack J, Draguhn A (2018) Respiration-Entrained Brain Rhythms Are Global but Often Overlooked. Trends Neurosci 41:186-197.

Tort ABL, Ponsel S, Jessberger J, Yanovsky Y, Brankack J, Draguhn A (2018) Parallel detection of theta and respiration-coupled oscillations throughout the mouse brain. Sci Rep 8:6432.

Vanderwolf CH (1969) Hippocampal electrical activity and voluntary movement in the rat. Electroencephalogr Clin Neurophysiol 26:407-418.

Wohr M, Borta A, Schwarting RK (2005) Overt behavior and ultrasonic vocalization in a fear conditioning paradigm: a dose-response study in the rat. Neurobiol Learn Mem 84:228-240.

Wohr M, Schwarting RK (2008) Maternal care, isolation-induced infant ultrasonic calling, and their relations to adult anxiety-related behavior in the rat. Behav Neurosci 122:310-330.

Wohr M, Scattoni ML (2013) Behavioural methods used in rodent models of autism spectrum disorders: current standards and new developments. Behav Brain Res 251:5-17.

Wu R, Liu Y, Wang L, Li B, Xu F (2017) Activity Patterns Elicited by Airflow in the Olfactory Bulb and Their Possible Functions. J Neurosci 37:10700-10711.

Yanovsky Y, Ciatipis M, Draguhn A, Tort AB, Brankack J (2014) Slow oscillations in the mouse hippocampus entrained by nasal respiration. J Neurosci 34:5949-5964.

Zelano C, Jiang H, Zhou G, Arora N, Schuele S, Rosenow J, Gottfried JA (2016) Nasal Respiration Entrains Human Limbic Oscillations and Modulates Cognitive Function. J Neurosci 36:12448-12467.

Zhong W, Ciatipis M, Wolfenstetter T, Jessberger J, Muller C, Ponsel S, Yanovsky Y, Brankack J, Tort ABL, Draguhn A (2017) Selective entrainment of gamma subbands by different slow network oscillations. Proc Natl Acad Sci U S A 114:4519-4524.

FIGURE LEGENDS

Figure 1 : A) Training and recording protocol. The animals were trained with 10 odor(20s)-Schock(1s) pairings. During the 1-min post-shock period, local field potentials were recorded together with ultrasonic vocalizations and behavior. 48h later, a retention test was carried out using 5 odor(20s) presentations during which the animal's freezing response was assessed. B) Definition of four experimental categories for data analysis. During the 1-min post-shock period, we defined blocks of USV corresponding to successive USV with less than 1s between each other. When the interval between two USV exceeded 1s, then a new block was defined (first row). The periods between USV blocks are considered as Silent periods. In parallel, the synchronized animal's behavior (Freezing or Escape) was detected, and four different combinations were obtained: USV Freezing, USV Escape, Silent Freezing, Silent Escape. For each combination, only segments longer than 1s were considered.

Figure 2: Repartition of the four defined categories and characterization of two 22-kHz USV types (n=22 rats). A) Mean (±SEM) proportion of each category per animal over the 1-min post-shock analysis period. B) Mean (±SEM) duration of the different categories and mean (±SEM) number of USV Freezing and USV Escape emitted during the 1-min post-shock period. C) Mean duration (±SEM) of the two USV subtypes. D) Mean frequency (±SEM) of the two USV subtypes. E) Mean intensity (±SEM) of the two USV subtypes. n=22 rats, * $p<5x10^{-2}$, ***$p<5x10^{-3}$. F) Correlation between the mean number of USV calls recorded during the 1-min post-shock period at training and the freezing score obtained during the retention test in response to the learned odor. * $p<5x10^{-2}$

677 **Figure 3:** Power Spectral Density (PSD) of local field potential signals and mean power in
678 delta (0-5Hz) and theta (5-15Hz) bands. The average PSD (±SEM) is represented on the left
679 part of the figure, and the delta and theta average power (±SEM) is represented on the right
680 part. BLA: basolateral amygdala (n=14), mPFC: medial prefrontal cortex (n=21) and PIR:
681 olfactory piriform cortex (n=20). * $p<5x10^{-2}$, ** $p<5x10^{-3}$, ***$p<5x10^{-4}$: significant difference
682 between same color-different pattern bars. $^{\$}$ $p<5x10^{-2}$, $^{\$\$}$ $p<5x10^{-3}$, $^{\$\$\$}$ $p<5x10^{-4}$: significant
683 difference between same pattern-different color bars.
684
685 **Figure 4:** Power Spectral Density (PSD) of local field potential signals and mean power in
686 gamma (40-80Hz) band. The average PSD (±SEM) is represented on the left part of the
687 figure, and the gamma average power (±SEM) is represented on the right part. BLA:
688 basolateral amygdala (n=14), mPFC: medial prefrontal cortex (n=21) and PIR: olfactory
689 piriform cortex (n=20). * $p<5x10^{-2}$, ** $p<5x10^{-3}$, ***$p<5x10^{-4}$: significant difference between
690 same color-different pattern bars. $^{\$}$ $p<5x10^{-2}$, $^{\$\$}$ $p<5x10^{-3}$, $^{\$\$\$}$ $p<5x10^{-4}$: significant difference
691 between same pattern-different color bars.
692
693 **Figure 5:** Characterization of respiratory frequency in the four experimental categories (n=22
694 rats). A) Individual examples of the respiratory signal. B) Probability Distribution Function
695 (PDF) of respiratory frequency. The distributions were obtained using a 0.33 Hz bin. Insert:
696 Average peak frequency (± SEM) in each category.
697
698 **Figure 6:** Covariation between delta and theta oscillatory frequencies and respiratory
699 frequency. A) Each graph represents the Power Spectral Density (PSD) of local field potential
700 (LFP) signals (Left Y axis, black curve) and the Probability Distribution Function (PDF) of

701 respiration (Right Y axis, red curve). The graphs were obtained from LFP signals recorded in
702 the medial prefrontal cortex in the four experimental categories (Silent Escape, USV Escape,
703 Silent Freezing, USV Freezing). B) 2D matrix histograms obtained from LFP signals recorded in
704 mPFC (n=21), basolateral amygdala (BLA, n=14) and olfactory piriform cortex (PIR, n=20), Y-
705 axis represents LFP frequency and X-axis respiratory frequency. The 2D histogram is
706 normalized so that the total sum is 1, and point density is represented on a color scale
707 ranging from blue to yellow as the point density increases.
708
709 **Figure 7:** Modulation of beta and gamma power by the phase of the respiratory cycle. A)
710 Individual traces representing from the top, respiratory signal, USV calls, raw local field
711 potential (LFP) signal recorded in the olfactory piriform cortex and its time frequency map (Y
712 axis: LFP signal frequency in Hz, X axis: time in ms). LFP signal power is represented using a
713 color scale going from blue to red as the power increases. The red vertical plain line
714 represents the transition between expiration and inspiration, while the red vertical dotted
715 line represents the transition between inspiration and expiration. B) Average time frequency
716 map centered on the normalized respiratory cycle, in the four experimental categories. The
717 red vertical dotted line represents the transition between inspiration and expiration phase
718 that was set at 0.4 (this value corresponds to the mean ratio between inspiration and
719 expiration over the four experimental categories). The white horizontal dotted line
720 represents the transition between beta and gamma bands.
721
722 **Figure 8:** Beta activity power time course throughout the normalized respiratory cycle in the
723 three recording sites and in the four experimental categories. Left side: Silent Freezing
724 versus USV Freezing, right side: Silent Escape versus USV Escape. The vertical dotted line on

each graph represents the transition between inspiration and expiration phase positioned at 0.4 (this value corresponds to the mean ratio between inspiration and expiration over the four experimental categories). BLA: basolateral amygdala (n=14), mPFC: medial prefrontal cortex (n=21) and PIR: olfactory piriform cortex (n=20).

Figure 9: Gamma activity power time course throughout the normalized respiratory cycle in the three recording sites and in the four experimental categories. Left side: Silent Freezing versus USV Freezing, right side: Silent Escape versus USV Escape. The vertical dotted line on each graph represents the transition between inspiration and expiration phase positioned at 0.4 (this value corresponds to the mean ratio between inspiration and expiration over the four experimental categories). BLA: basolateral amygdala (n=14), mPFC: medial prefrontal cortex (n=21) and PIR: olfactory piriform cortex (n=20).

Figure 10: Schematic summary of the data obtained during Silent Freezing and USV Freezing. During Silent Freezing, delta frequency covaries with nasal respiratory frequency. In addition, power in the beta band for the piriform cortex and in the gamma band for the three recording sites is modulated in phase with respiration, with higher beta and gamma power during inspiration than expiration. USV Freezing emission coincides with a decrease in theta power and an increase in delta and gamma power. In parallel, a deep slow-down of respiratory frequency is observed, with the uncoupling between delta frequency and respiratory frequency. Furthermore, a reorganization of beta and gamma activity power during the respiratory cycle occurs, with increased beta power in the piriform cortex during the first half of expiration phase, and increased gamma power in the three recording sites

748 during the second half of expiration. mPFC: medial prefrontal cortex, BLA: basolateral
749 amygdala, PIR: piriform cortex, LFP: local field potentials

750

751 **TABLE LEGENDS**

752

753 **Table 1:** Delta and Theta activity mean power statistical data: ANOVA analysis (upper table)
754 and p values for post-hoc comparisons (lower table).
755 * : $p \leq 5x10^{-2}$, ** : $p \leq 5x10^{-3}$, *** : $p \leq 5x10^{-4}$.

756

757 **Table 2:** Beta band mean power values (+/- sem) in the three recording sites (upper table),
758 ANOVA analysis (middle table), and p values for post-hoc comparisons (lower table).
759 * : $p \leq 5x10^{-2}$, ** : $p \leq 5x10^{-3}$, *** : $p \leq 5x10^{-4}$.

760

761 **Table 3:** Gamma band mean power statistical data in the three recording sites: ANOVA
762 analysis (upper table) and p values for post-hoc comparisons (lower table).
763 * : $p \leq 5x10^{-2}$, ** : $p \leq 5x10^{-3}$, *** : $p \leq 5x10^{-4}$.

764

765 **Table 4:** Beta (upper table) and Gamma (lower table) bands maximum power throughout the
766 respiratory cycle, ANOVA analysis. * : $p \leq 5x10^{-2}$, ** : $p \leq 5x10^{-3}$, *** : $p \leq 5x10^{-4}$.

767 **EXTENDED DATA**

768

769 **Figure 1-1:** Areas targeted by the electrodes (light orange areas) in the three recording sites.
770 Numbers at the bottom indicate the relative position of coronal slices from bregma (Adapted

771 from Paxinos and Watson, 2007). mPFC: medial prefrontal cortex (n=21), PIR: olfactory
772 piriform cortex (n=20) and BLA: basolateral amygdala (n=14).
773
774 **Figure 6-1:** Examples of raw traces obtained in the same animal in the three recording sites
775 and the four experimental categories. Each panel represents from the top : ultrasonic
776 vocalizations (USV) calls (for the panels on the right), raw respiratory signal, and local field
777 potential signals recorded in the basolateral amygdala (BLA), medial prefrontal cortex
778 (mPFC) and olfactory piriform cortex (PIR).
779
780 **Figure 7-1:** Modulation of beta and gamma power by the phase of the respiratory cycle.
781 Average time frequency maps centered on the normalized respiratory cycle, in the three-
782 recorded structures (along the vertical axis) and the four experimental categories (along the
783 horizontal axis). On each graph, the red vertical dotted line represents the transition
784 between inspiration and expiration that was set at 0.4, and the white horizontal dotted line
785 represents the transition between beta and gamma bands. BLA: basolateral amygdala
786 (n=14), mPFC: medial prefrontal cortex (n=21) and PIR: olfactory piriform cortex (n=20).
787

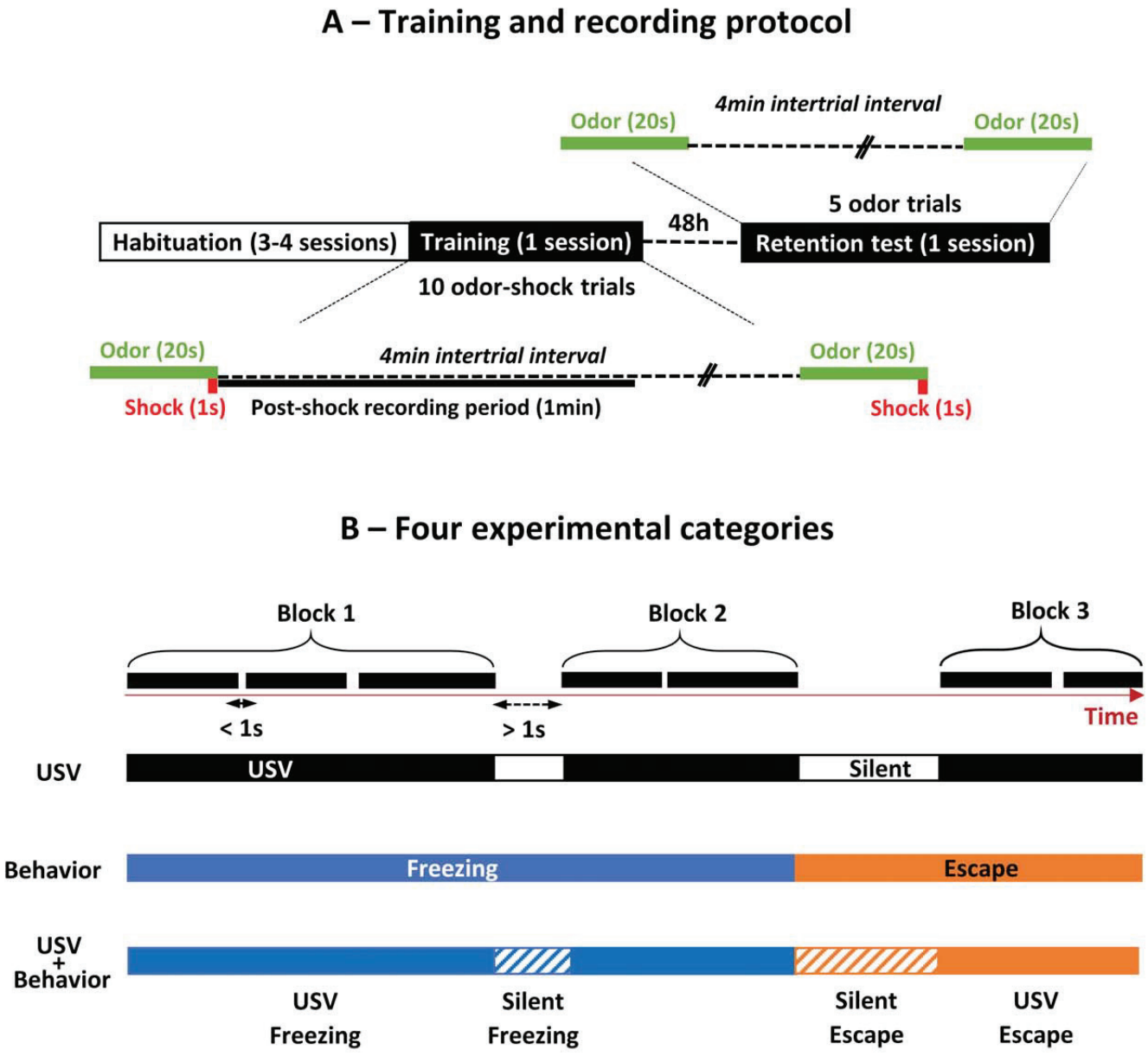

Figure 1

A

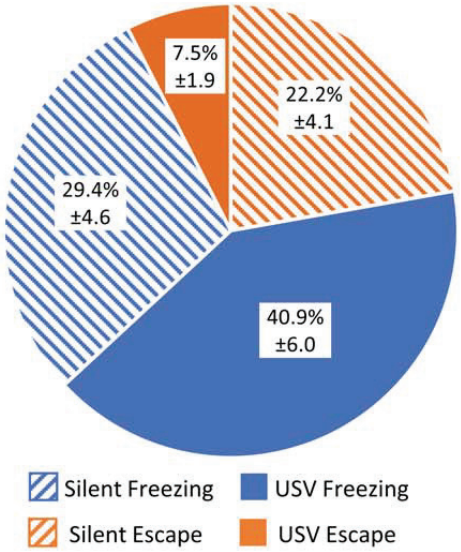

B

Experimental category	Mean Behavior duration (s)/1 min	Mean USV Nb/1min
USV Freezing	24.5±3.6	16±2
Silent Freezing	17.6±2.7	
USV Escape	4.5±1.2	4±1
Silent Escape	13.3±2.4	

C

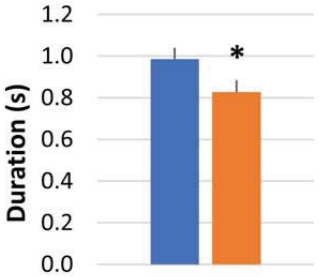

D

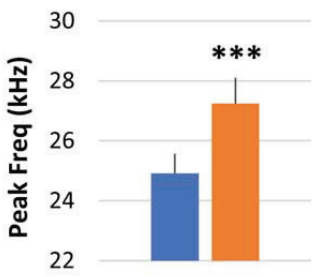

E

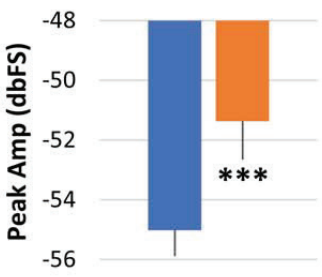

F

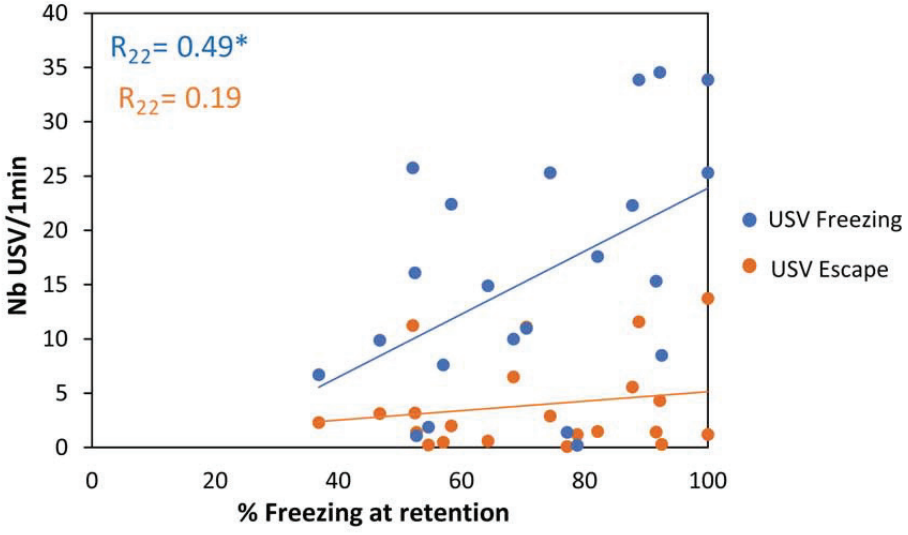

Figure 2

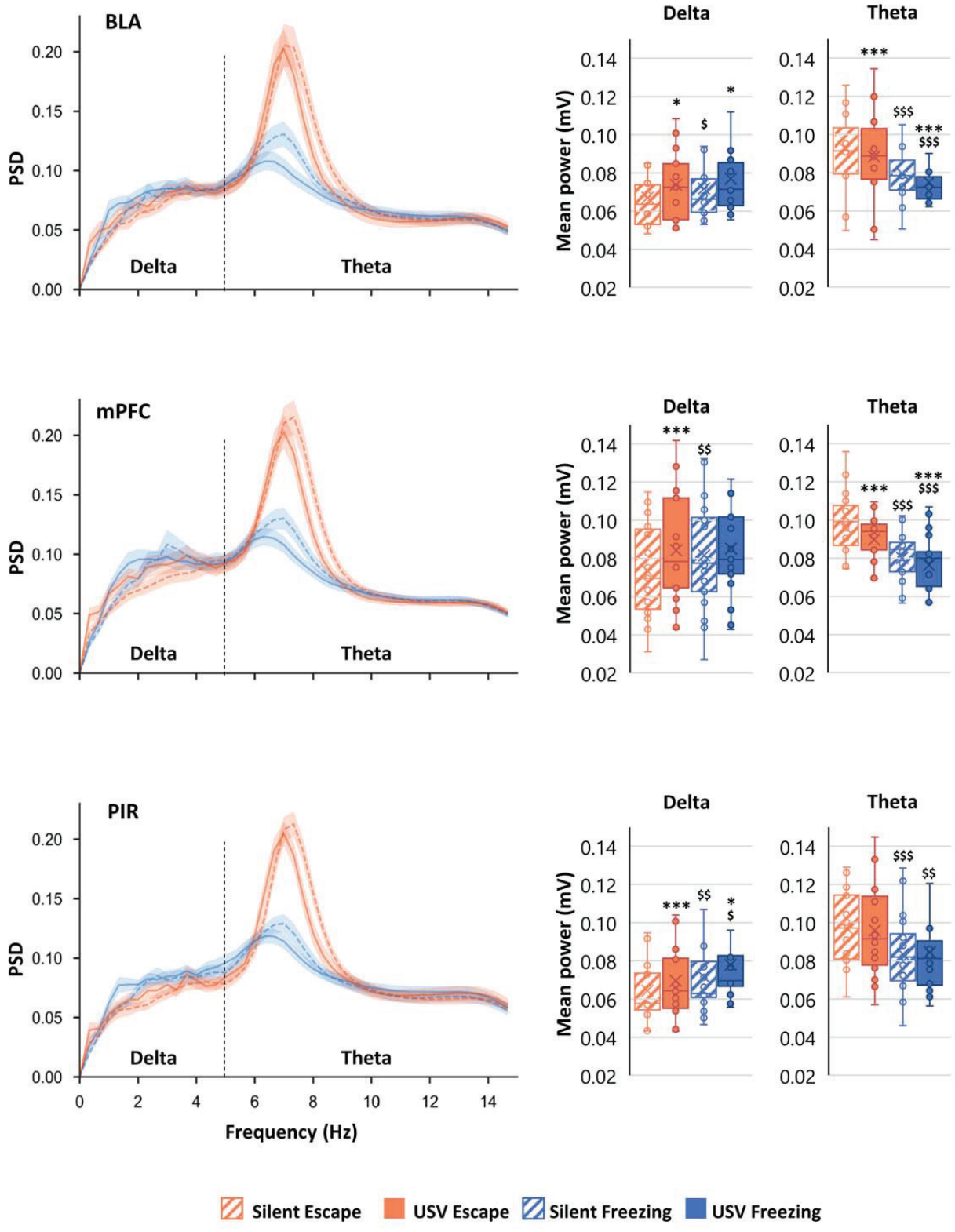

Figure 3

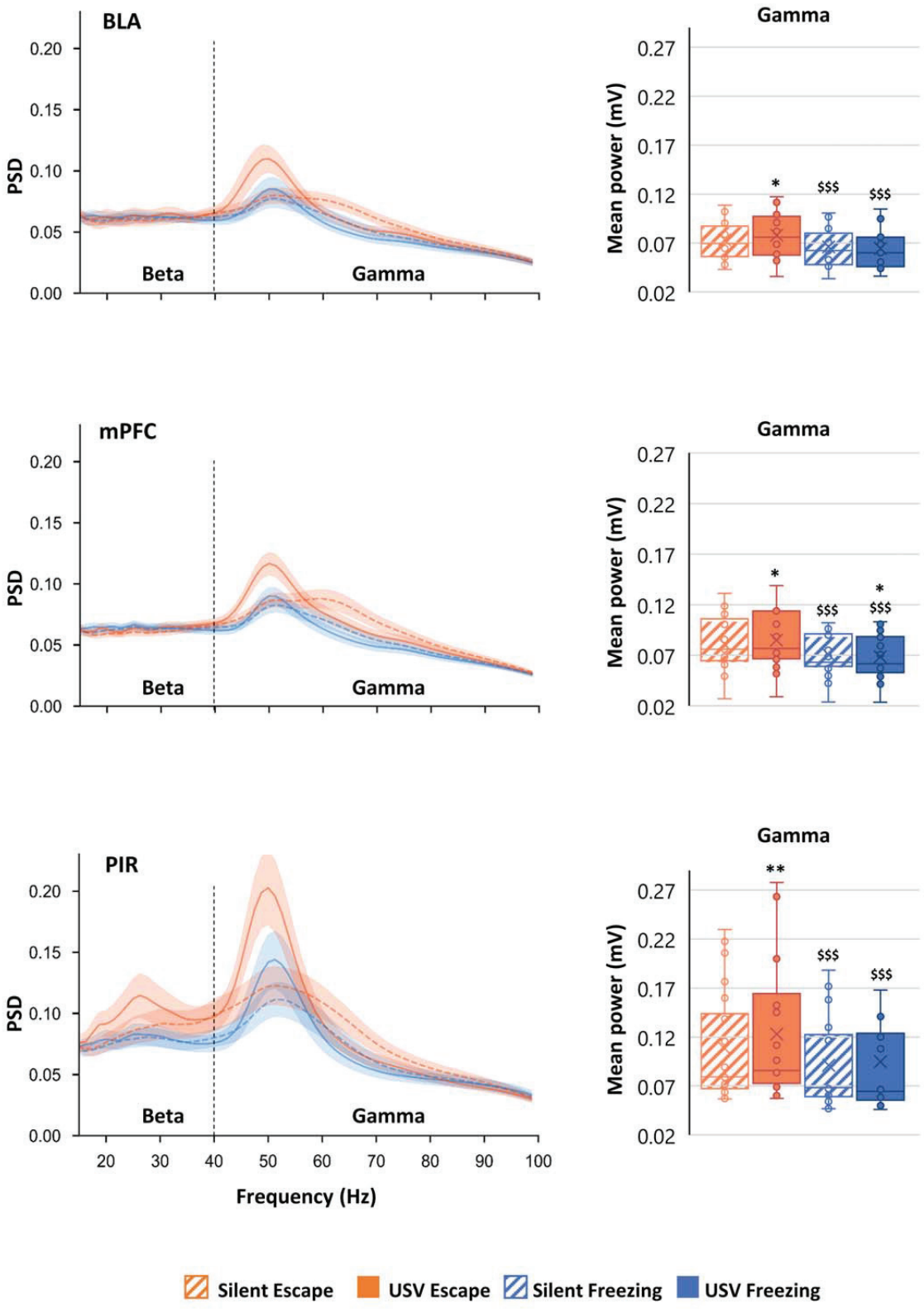

Figure 4

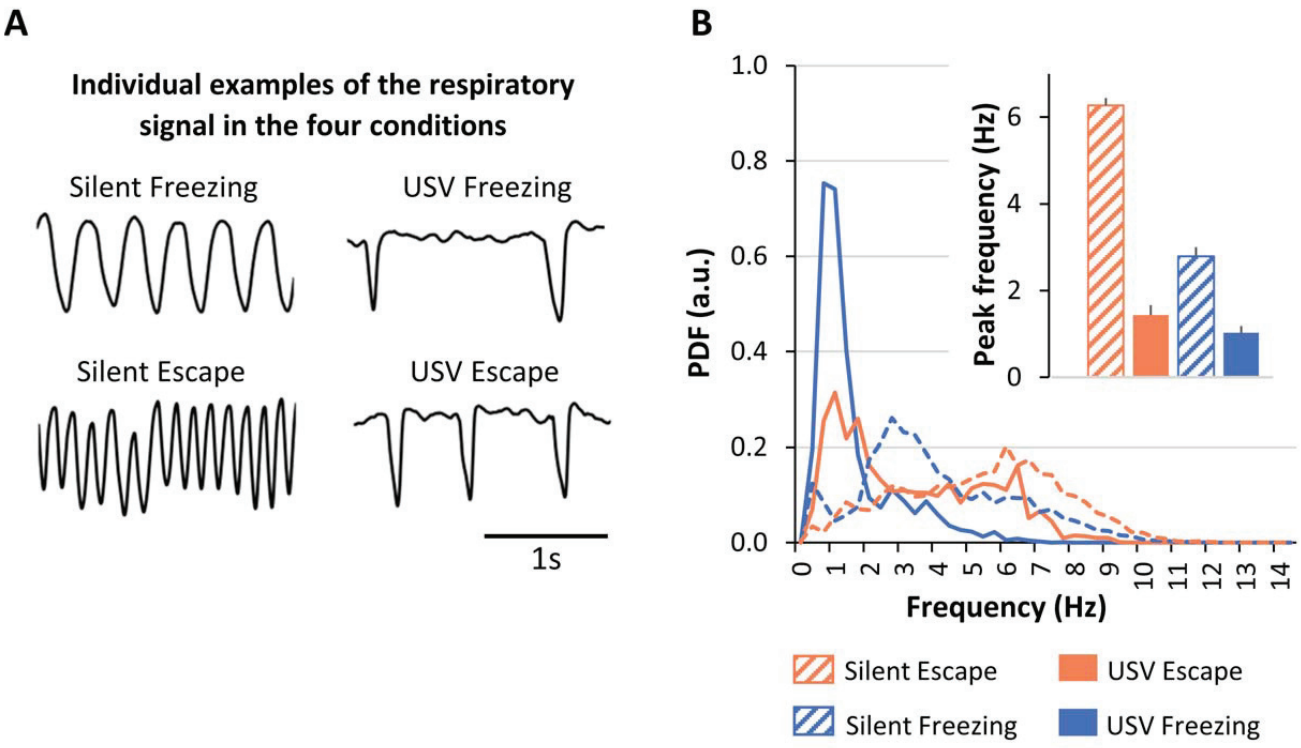

Figure 5

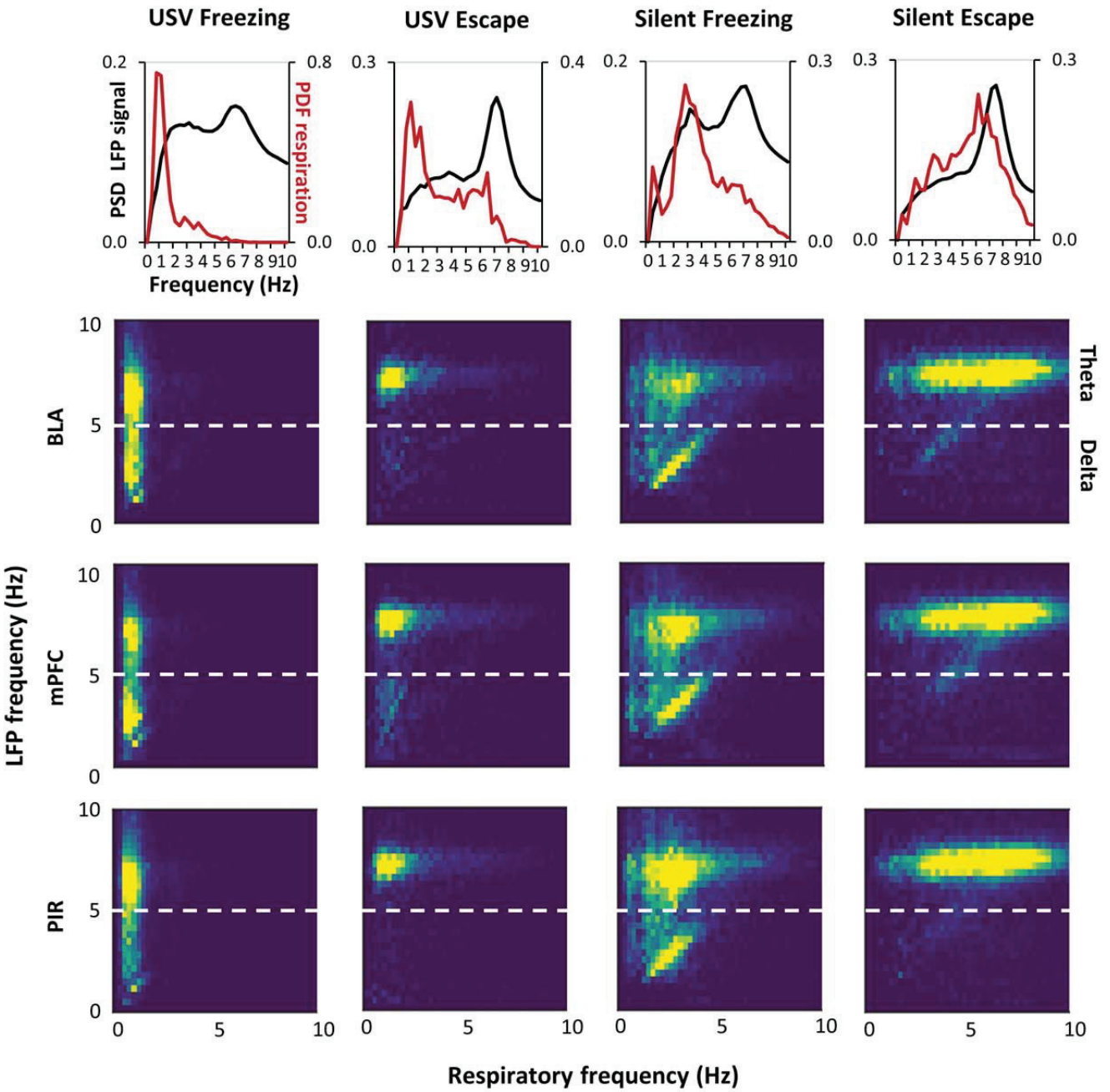

Figure 6

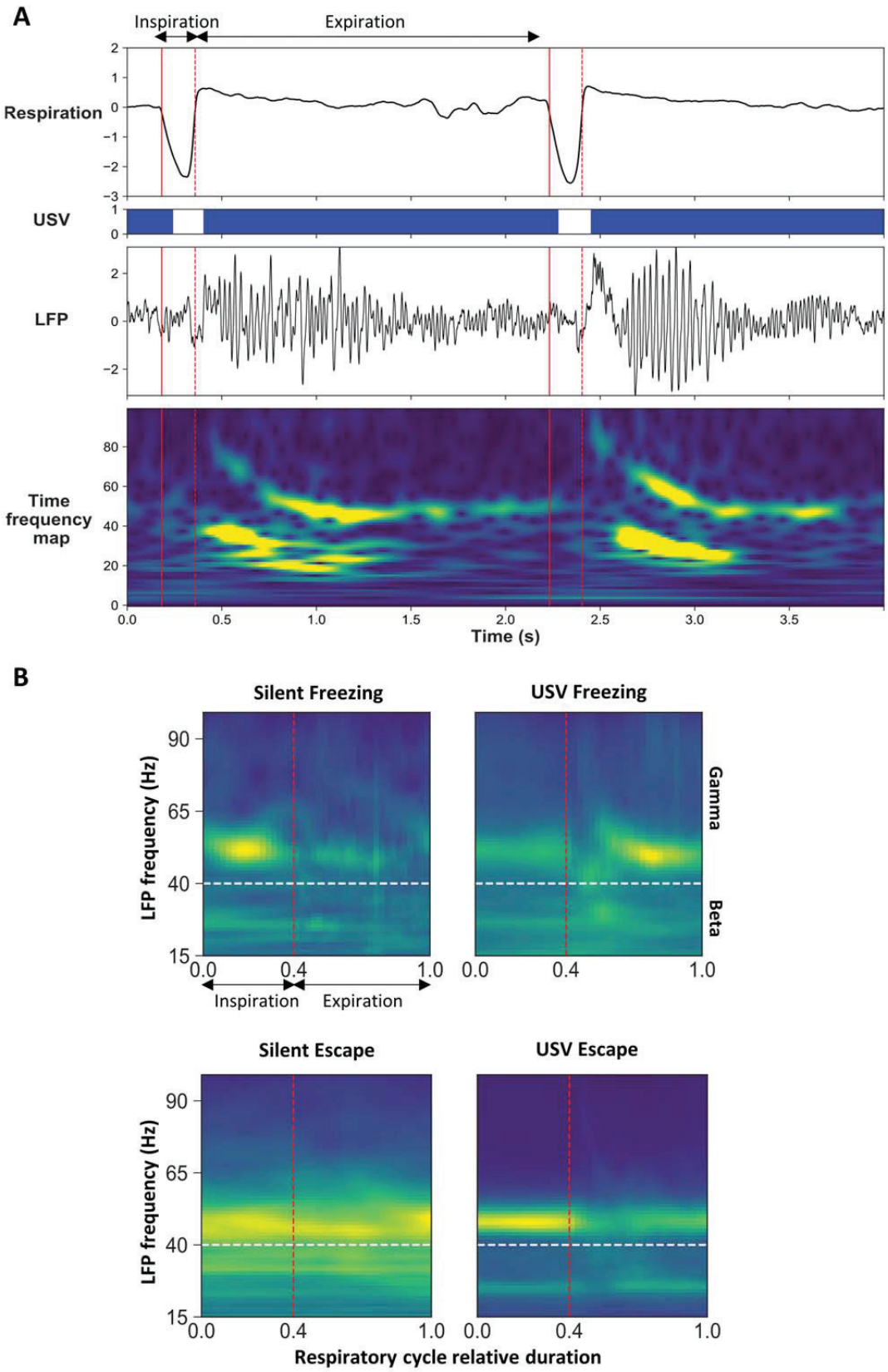

Figure 7

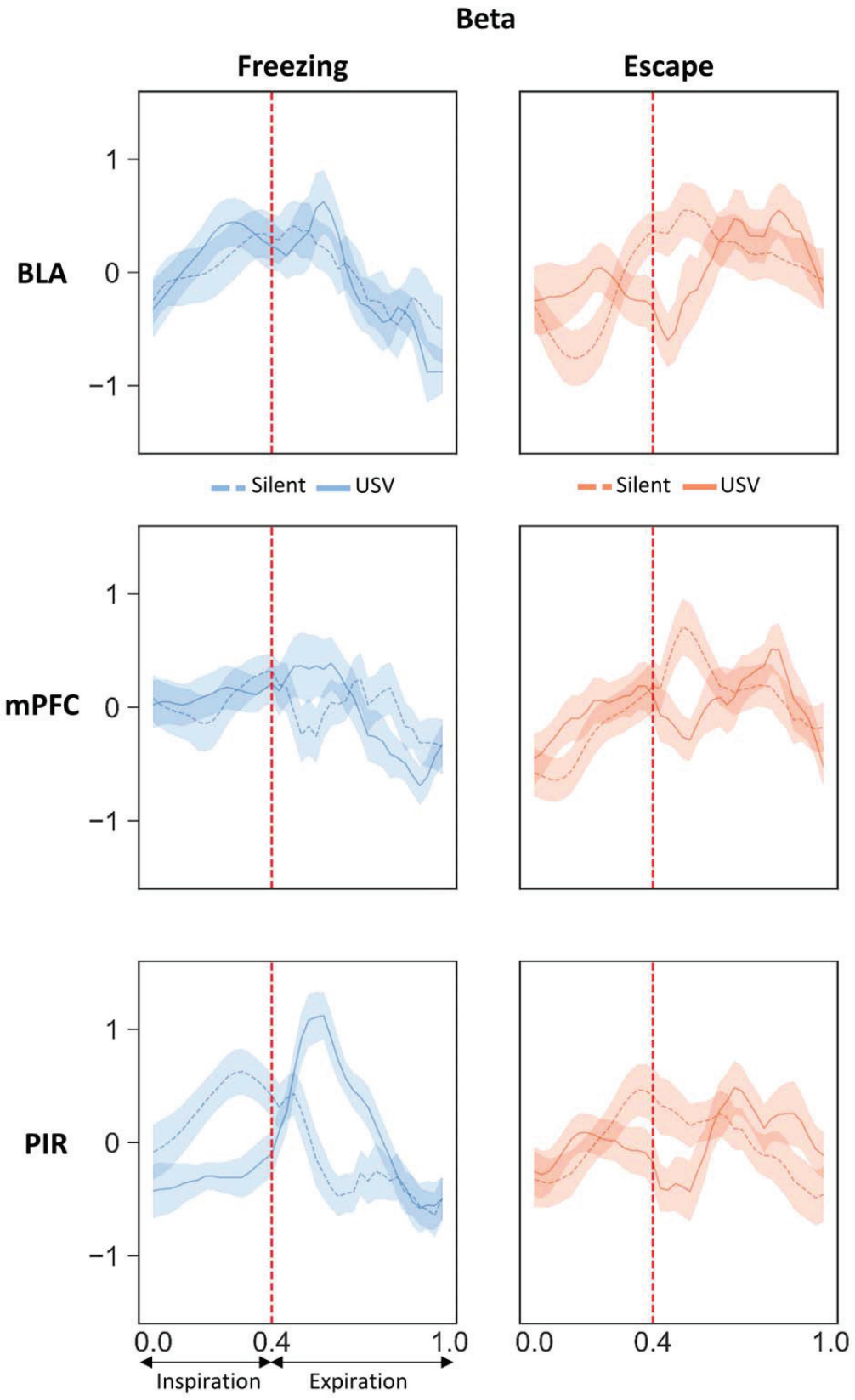

Figure 8

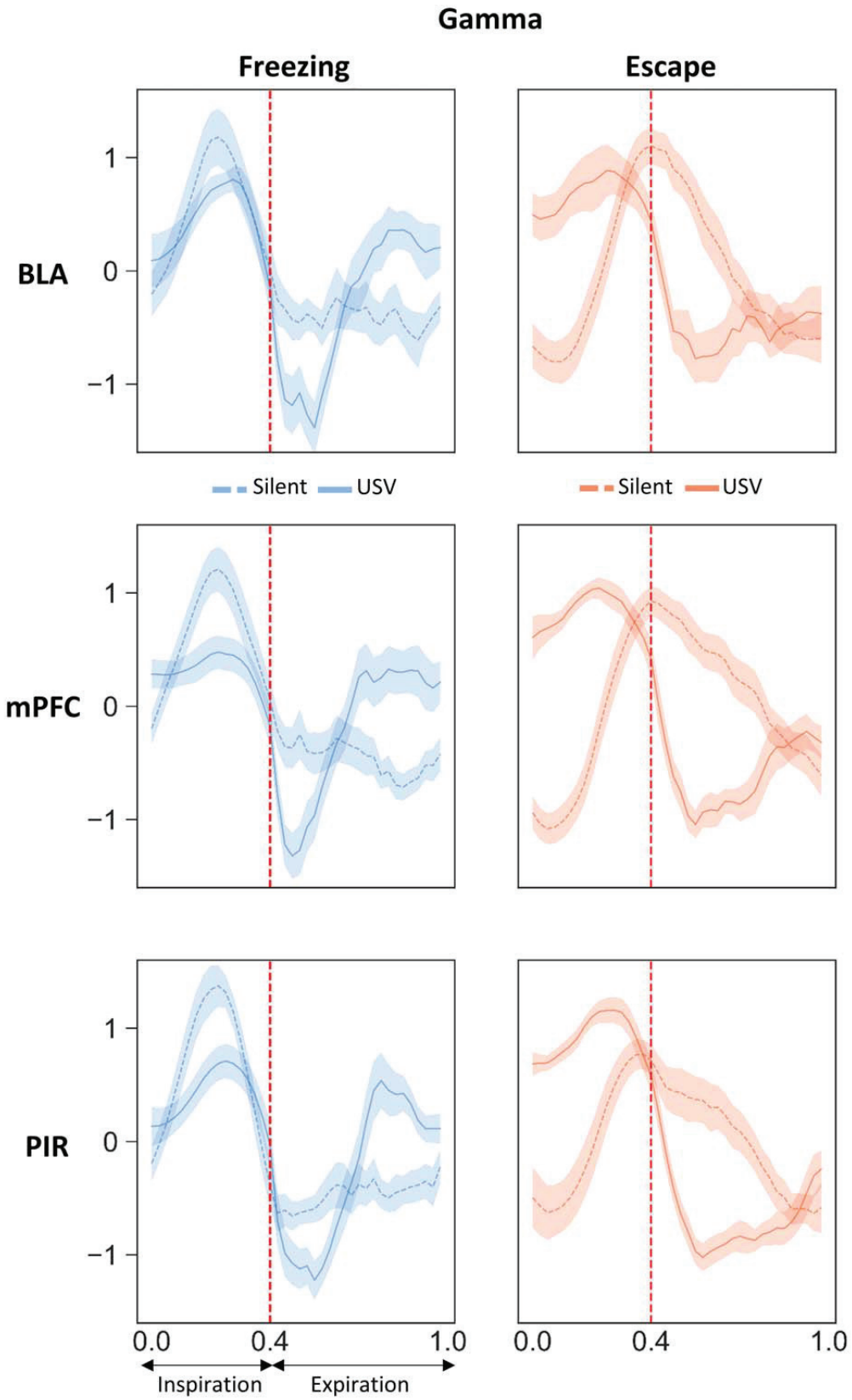

Figure 9

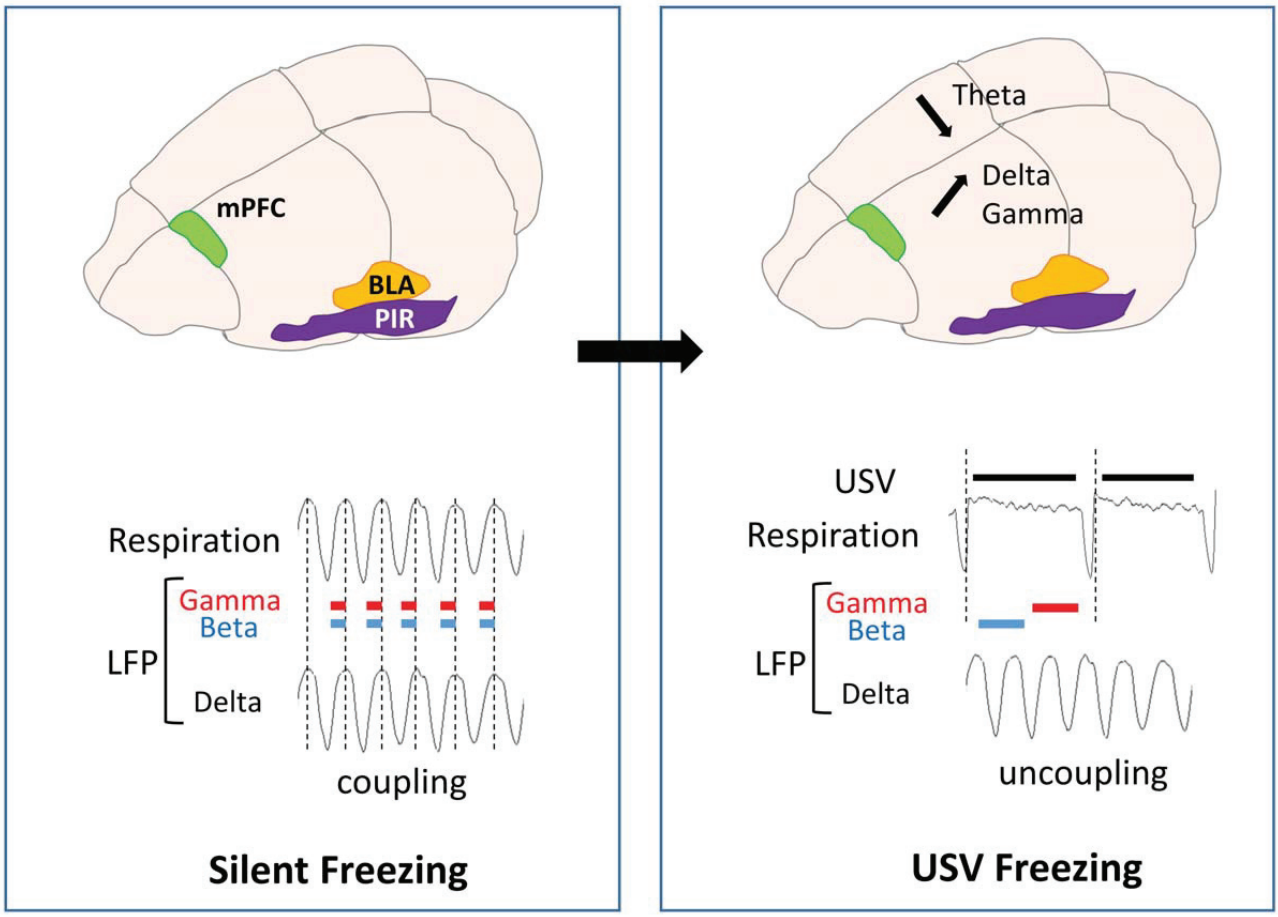

Figure 10

Oscillatory Band	Structure	Factor	F (ddl)	F value	P value
Delta Mean power	BLA	USV	1,13	17.97	$1x10^{-3}$**
		Behavior		11.26	$5x10^{-3}$**
		USVxBehavior		0.62	0.4
	mPFC	USV	1,20	17.56	$5x10^{-4}$***
		Behavior		5.70	$3x10^{-2}$*
		USVxBehavior		9.28	$6x10^{-3}$*
	PIR	USV	1,19	13.25	$2x10^{-3}$**
		Behavior		33.22	$1x10^{-5}$***
		USVxBehavior		0.15	0.7
Theta Mean power	BLA	USV	1,13	18.82	$8x10^{-4}$**
		Behavior		28.43	$1x10^{-4}$***
		USVxBehavior		0.01	0.9
	mPFC	USV	1,20	27.77	$4x10^{-5}$***
		Behavior		114.73	$1x10^{-5}$***
		USVxBehavior		2.13	0.2
	PIR	USV	1,19	0.01	0.9
		Behavior		61.99	$1x10^{-5}$***
		USVxBehavior		0.70	0.4

Oscillatory Band	Structure	Silent Freezing vs Silent Escape	USV Freezing vs USV Escape	Silent Freezing vs USV Freezing	Silent Escape vs USV Escape
Delta Mean power	BLA	$3x10^{-2}$*	0.1	$5x10^{-3}$*	$6x10^{-3}$*
	mPFC	$1x10^{-3}$***	0.7	0.1	$7x10^{-5}$***
	PIR	$8x10^{-4}$**	$1x10^{-3}$*	$3x10^{-2}$*	$1x10^{-4}$***
Theta Mean power	BLA	$7x10^{-6}$***	$8x10^{-4}$*	$2x10^{-2}$*	$1x10^{-4}$***
	mPFC	$1x10^{-6}$***	$1x10^{-6}$***	$6x10^{-3}$*	$1x10^{-4}$***
	PIR	$1x10^{-6}$***	$1x10^{-3}$**	0.7	0.5

Table 1

	Silent Escape	USV Escape	Silent Freezing	USV Freezing
BLA	0.062±0.005	0.064±0.005	0.062±0.005	0.063±0.004
mPFC	0.062±0.003	0.064±0.003	0.063±0.003	0.064±0.003
PIR	0.087±0.010	0.099±0.007	0.077±0.007	0.079±0.013

Structure	Factor	F (ddl)	F value	p value
BLA	USV	1,13	2.24	0.2
	Behavior		0.11	0.7
	USVxBehavior		0.40	0.5
mPFC	USV	1,20	11.60	$3x10^{-3}$**
	Behavior		0.53	0.5
	USVxBehavior		2.43	0.1
PIR	USV	1,19	9.04	$7x10^{-3}$*
	Behavior		6.06	$2x10^{-2}$*
	USVxBehavior		9.58	$6x10^{-3}$*

Structure	Silent Freezing vs Silent Escape	USV Freezing vs USV Escape	Silent Freezing vs USV Freezing	Silent Escape vs USV Escape
BLA	0.9	0.6	0.2	0.3
mPFC	0.1	0.9	$1x10^{-2}$*	$1x10^{-2}$*
PIR	0.1	$1x10^{-2}$*	0.5	$2x10^{-3}$**

Table 2

Structure	Factor	F (ddl)	F value	p value
BLA	USV	1,13	1.53	0.2
	Behavior		78.54	$1x10^{-5}$***
	USVxBehavior		6.99	$2x10^{-2}$*
mPFC	USV	1,20	0.80	0.4
	Behavior		59.79	$1x10^{-5}$***
	USVxBehavior		15.69	$8x10^{-4}$**
PIR	USV	1,19	6.29	$2x10^{-2}$*
	Behavior		31.94	$2x10^{-5}$***
	USVxBehavior		11.74	$3x10^{-2}$*

Structure	Silent Freezing vs Silent Escape	USV Freezing vs USV Escape	USV Freezing vs Silent Freezing	USV Escape vs Silent Escape
BLA	$1x10^{-6}$***	$2x10^{-5}$***	0.1	$2x10^{-2}$*
mPFC	$5x10^{-6}$***	$1x10^{-6}$***	$3x10^{-2}$*	$9x10^{-3}$*
PIR	$6x10^{-4}$**	$4x10^{-6}$***	0.4	$9x10^{-4}$**

Table 3

Beta band		Freezing			Escape		
Structure	**Factor**	**F (ddl)**	**F value**	**p value**	**F (ddl)**	**F value**	**p value**
BLA	**Respiratory cycle time**	39,507	2.32	$2x10^{-5}$***	39,507	2.35	$1x10^{-5}$***
	USV	1,13	2.4	0.1	1,13	0.11	0.7
	Respiratory cycle time x USV	39,507	1.05	0.4	39,507	1.29	0.1
mPFC	**Respiratory cycle time**	39,780	1.53	$2x10^{-2}$*	39,780	2.04	$2x10^{-4}$***
	USV	1,20	3.16	0.1	1,20		
	Respiratory cycle time x USV	39,780	1.09	0.3	39,780	1.99	0.2
PIR	**Respiratory cycle time**	39,741	5.72	$1x10^{-7}$***	39,741	1.56	$2x10^{-2}$*
	USV	1,19	0.15	0.70	1,19	0.62	0.4
	Respiratory cycle time x USV	39,741	2.65	$4x10^{-7}$***	39,741	1.30	0.1

Gamma band		Freezing			Escape		
Structure	**Factor**	**F (ddl)**	**F value**	**p value**	**F (ddl)**	**F value**	**p value**
BLA	**Respiratory cycle time**	39,507	11.06	$1x10^{-6}$***	39,507	7.58	$1x10^{-7}$***
	USV	1,13	0.41	0.5	1,13	3.79	$7x10^{-2}$
	Respiratory cycle time x USV	39,507	5.28	$1x10^{-6}$***	39,507	3.65	$1x10^{-7}$***
mPFC	**Respiratory cycle time**	39,780	11.65	$1x10^{-6}$***	39,780	22.08	$1x10^{-7}$***
	USV	1,20	1.05	0.3	1,20	6.95	$2x10^{-2}$*
	Respiratory cycle time x USV	39,780	5.03	$1x10^{-6}$***	39,780	5.64	$1x10^{-7}$***
PIR	**Respiratory cycle time**	39,741	13.36	$1x10^{-6}$***	39,741	16.11	$1x10^{-7}$***
	USV	1,19	0.27	0.6	1,19	9.03	$7x10^{-3}$*
	Respiratory cycle time x USV	39,741	7.72	$1x10^{-6}$***	39,741	4.31	$1x10^{-7}$***

Table 4